Urban green space and albedo impacts on surface temperature across seven United States cities

Ian A. Smith[1*], M. Patricia Fabian[2], Lucy R. Hutyra[1]

[1]*Boston University, Department of Earth & Environment, 685 Commonwealth Ave., Boston, MA, 02215, USA*
[2]*Boston University, Department of Environmental Health, 715 Albany St., Boston, MA, 02118, USA*

*Corresponding Author: Ian A. Smith (iasmith@bu.edu)

Key Words: Urban greening, white roofs, albedo, surface temperature, urban heat island, climate change, climate adaptation, heat exposure

Abstract

Extreme heat represents a growing threat to public health, especially across the densely populated, developed landscape of cities. Climate adaptation strategies that aim to manage urban microclimates through purposeful design can reduce the heat exposure of urban populations, however, it is unclear how the temperature impacts of urban green space and albedo vary across cities and background climate. This study quantifies the sensitivity of surface temperature to landcover characteristics tied to two widely used climate adaptation strategies, urban greening and albedo manipulation (e.g. white roofs), by combining long-term remote sensing observations of land surface temperature, albedo, and moisture with high-resolution landcover datasets in a spatial regression analysis at the census block scale across seven United States cities. We find tree cover to have an average cooling impact of -0.089 K per % cover, which is approximately four times stronger than the average grass cover cooling impact of -0.021 K per % cover. Variability in the magnitude of grass cover cooling impacts was primarily a function of vegetation moisture content, with the Land Surface Water Index (LSWI) explaining 89% of the variability in grass cover cooling impacts across cities. Variability in tree cover cooling impacts was primarily a function of sunlight and vegetation moisture content, with solar irradiance and LSWI explaining 97% of the cooling variability across cities. Albedo cooling impacts were consistent across cities with an average cooling impact of -0.187 K per increase of 0.01. While these interventions are broadly effective across cities, there are critical regional trade-offs between vegetation cooling efficiency, irrigation requirements, and the temporal duration and evolution of the cooling benefits. In warm, arid cities, high albedo surfaces offer multifaceted benefits such as cooling and water conservation, whereas temperate, mesic cities likely benefit from a combination of strategies, with greening efforts targeting highly paved neighborhoods.

Smith, I.A., Fabian, P.M., Hutyra, L.R., Landcover composition and albedo impacts on urban surface temperature across seven United States cities: Towards optimal climate sensitive design, Science of the Total Environment, 857: 159663, 2023.

1. Introduction

In the current era of multifaceted global change, urbanization and anthropogenic climate forcing are working synergistically to expose much of the Earth's population to extreme high temperatures. Between 1995 and 2014, the global average surface temperature was 0.85 °C warmer than the preindustrial average and is projected to continue warming throughout the 21st century, with extreme heat events expected to occur more frequently and with greater intensity (IPCC 2021). At the same time, humanity continues to experience an unprecedented shift towards urban living, with more than half of the global population now living in the built environment of cities (Grimm et al. 2008) where the combined effects of global warming and urban heat islands (Oke 1982) exacerbate the health risks associated with heat waves (Zhou et al. 2022).

At the nexus of urbanization and climate change lies a growing threat to public health as moderate and extreme heat exposure is a well-documented contributor to human morbidity and mortality (Sarofim et al. 2016). In the United States, more deaths are attributed to heat exposure than to any other natural disaster (Bell et al. 2016). Furthermore, the public health burden of heat exposure includes a multitude of non-fatal exposure consequences such as adverse pregnancy outcomes, dehydration, loss of labor productivity, and decreased academic achievement (Bekkar et al. 2020, Heal & Park 2016; Zivin & Neidell 2014; Park et al. 2020). Heat disproportionately impacts vulnerable populations such as older adults, outdoor workers, people of color, and residents of low-income households (Sarofim et al. 2016, US EPA 2021). Thus, in addition to tackling the global climate crisis, there is an urgent need for cities to consider climate adaptation strategies promoting equitable, sustainable, and heat resilient urban ecosystems.

Numerous urban design strategies have been proposed to minimize heat exposure to urban residents including reduction of anthropogenic heat emissions, access to cooling centers, and strategic development of wind corridors (Leal Filho et al. 2017). Here we focus on two of the most common and well-founded urban design strategies, urban greening and the incorporation of high albedo surfaces such as white roofs, which are intended to manipulate the storage, transformation, and exchange of incoming solar radiation to reduce surface temperatures in cities.

Urban greening for heat mitigation refers to the expansion of vegetation, particularly trees, to shade the surface from sunlight and increase evapotranspiration such that more of the incoming solar energy is transferred to the atmosphere via latent, rather than sensible heat. Variation in the capacity of urban versus rural surfaces to evaporate water is a primary driver of extreme daytime urban temperatures (Carlson and Boland 1978; Taha 1997; Li et al. 2019), however, the addition of greenspace to an otherwise impervious surface-dominated landscape can increase the potential daytime latent heat flux in cities (Zipper et al. 2017; Winbourne et al. 2020; Smith et al. 2021). Shading has also been demonstrated to be a prominent cooling mechanism of trees in cities, particularly on very hot days when soils dry (Rahman et al. 2018). Field studies (Wang et al. 2017; Ziter et al. 2019) and remote sensing studies (Tiangco et al. 2008) find supporting evidence for vegetation as an effective heat mitigation measure in cities.

The marginal impact (sometimes called ‘cooling efficiency’; Zhou et al. 2017) of green space on temperature describes the temperature change associated with a one-unit (e.g. 1% of green space) increase of vegetated land cover. Quantifying the marginal impacts of land cover on temperature provides a metric for cities to evaluate the potential for urban greening initiatives to reduce temperatures. Furthermore, exploring the variability in green space marginal impacts across cities can elucidate the environmental drivers governing the magnitude of vegetation cooling

impacts. Numerous studies have quantified the marginal impacts of vegetation on land surface temperature in United States cities (Weng et al. 2006, Zhou et al. 2011, Myint et al. 2015, Zhou et al. 2017, Zhang et al. 2019, Wang et al. 2019, Wang et al. 2020, Wang et al. 2022), however, studies that separate the impact of different forms of green space (e.g. grass cover versus tree cover) and studies exploring the variability in marginal cooling impacts across cities are limited.

Cool roofs and cool pavements, defined as surfaces with a high albedo, have also been implemented as a means to alleviate excessive urban heat (e.g. NYC CoolRoofs 2022) by redirecting the largest influx of energy to the land surface (incoming shortwave radiation; Oke 1988). While there is evidence that cool pavements at the ground level may negatively impact pedestrian thermal comfort during the daytime (Lynn et al. 2009, Erell et al. 2014, Taleghani et al. 2016), high albedo coatings on rooftops represent a pathway for increasing the surface albedo of cities while simultaneously avoiding increases in the radiative load of pedestrians. Roofs are a major facet of the built environment and play an important role in the surface energy balance due to their direct exposure to the sun and sky. Typical roofing materials tend to be strong absorbers of solar radiation (Oke et al. 2017) and because they are meant to protect the contents of buildings from infiltration, they are generally designed to remain dry and divert rainfall to gutters and drainage pipes. Consequently, the excess available energy fueled by absorption of incoming solar radiation is almost entirely shed as sensible, rather than latent heat (Oke et al. 2017). Increased white roof fractions in cities have been demonstrated to be an effective method of reducing surface and near-surface urban heat islands (Oleson et al. 2010; Jacobsen & Ten Hoeve 2012; Li et al. 2014), but have rarely been simultaneously considered with urban greening.

Cities across the United States are recognizing the need for climate adaptation measures (Shi et al. 2015) and adaptation efforts have expanded substantially in recent years (Easterling et al.

2018). The adaptive capacity of cities, however, is limited by knowledge gaps in our understanding of the marginal impacts of tree cover, grass cover, and albedo on temperature dynamics within cities, the influence of management practices such as irrigation on vegetation cooling efficiency, and the environmental variables governing the effectiveness of various strategies across cities. The cooling efficiency of urban design strategies likely varies within and across cities due to differences in proximate landcover composition and background climates, highlighting the need for improved understanding of observed greening and albedo cooling impacts.

In situ monitoring of air temperature within cities is generally limited to a relatively small number of monitoring stations that fail to provide sufficient spatial coverage for urban land use planning (Zhou et al. 2018). Satellite remote sensing of land surface temperature, however, offers consistent, repeatable, and spatially comprehensive observations of the urban thermal condition. This study combines high resolution spatial datasets of landcover with satellite-derived maps of surface temperature, surface moisture, and albedo to estimate the impact of land cover composition and albedo on surface temperature at the census block level in seven United States cities using a spatial regression analysis. The analysis aims to 1) quantify differences in tree versus grass cover cooling impacts within and across cities, 2) identify environmental drivers governing tree and grass cover cooling efficiency, 3) explore differences in the marginal cooling impacts of irrigated versus non-irrigated grass cover in an arid city, and 4) quantify the sensitivity of surface temperature to albedo across cities. This research deepens our understanding of the joint impacts of urban greening and albedo on surface temperatures, elucidates climatic drivers of vegetation cooling potential, and provides important information for city planners hoping to improve heat resiliency and preparedness for a changing climate through landscape (re)development decisions.

2. Methods

136 *2.1 Study sites and land cover data*

137 The seven US cities included in the analysis are Boston, Massachusetts; Charlotte, North
138 Carolina; Chicago, Illinois; Washington, District of Columbia (DC); Durham, North Carolina; San
139 Diego, California; and San Jose, California (Table 1; Figure 1). Cities were selected due to the
140 availability of high resolution (< 1 meter), consistent land cover datasets produced by the
141 University of Vermont Spatial Analysis Laboratory and acquired via the US Department of
142 Agriculture Research Date Archive (UVM SAL 2012; UVM SAL 2013a; UVM SAL 2013b; UVM
143 SAL 2016; UVM SAL 2017a; UVM SAL 2017b; UVM SAL 2020). The UVM SAL mapped
144 seven land cover classes for each city, including tree canopy, shrubs/grass, bare land, water,
145 buildings, roads, and other paved surfaces (Figure 2A-C). In San Jose, grass was further partitioned
146 as irrigated and non-irrigated (UVM SAL 2012). Land cover maps were created using a
147 combination of LiDAR, multispectral orthoimagery from the National Agriculture Imagery
148 Program, and ancillary GIS data sources. Land cover was mapped using automated object-based
149 image analysis techniques to group pixels into meaningful objects based on spectral and spatial
150 properties before a detailed manual review of the dataset was carried out to correct all observable
151 errors (UVM SAL 2012). Prior to our analysis, a 100-meter buffer surrounding all water bodies
152 was applied to exclude (mask) the areas immediately surrounding water to minimize misattribution
153 of landcover impacts on surface temperature due to the presence of water.

154 *2.2 Surface temperature data*

155 Land surface temperature maps (Figure 2J-L) were created with the surface temperature layer
156 from the Landsat 7 Level 2 Collection 2 Tier 1 Science Product (Masek et al. 2006) which was
157 acquired and processed with Google Earth Engine (Gorelick et al. 2017). Surface temperature data
158 is provided at 30-meter spatial resolution with images acquired every 16 days and is estimated

159 from Landsat thermal infrared bands using the top-of-atmosphere (TOA) reflectance, TOA
160 brightness temperature, Advanced Spaceborne Thermal Emission and Reflection Radiometer
161 (ASTER) emissivity data, ASTER Normalized Difference Vegetation Index (NDVI) data, and
162 atmospheric geopotential height, specific humidity, and air temperature provided by reanalysis
163 data. Under ideal clear sky conditions, the root mean square error of the Landsat surface
164 temperature product has been estimated to be <1 K (Laraby & Schott 2018). To reduce uncertainty
165 associated with surface temperature estimation, all images with <80% cloud cover collected during
166 June, July, and August (JJA) of the five years prior to the year depicted by each city's landcover
167 map were downloaded, filtered using the C Function of Mask algorithm (CFMASK ; Zhu &
168 Woodcock 2012) to only include pixels with clear sky conditions, and composited by calculating
169 the mean pixel surface temperature value across all images to create a raster representative of the
170 mean JJA clear sky surface temperatures during the sunlit Landsat overpass time across each city.
171 On average, each pixel had a clear sky observation in 70.7% of images used to create the raster
172 composites, with 95.0% of pixels having a clear sky observation in at least 50% of images used to
173 create the raster composites. An inventory of all Landsat images used in this analysis can be found
174 in SI Table 1. Landsat 7 imagery is used throughout the analysis to ensure consistency in the
175 sensors used for data collection and to allow for albedo estimation using methods derived for the
176 Enhanced Thematic Mapper Plus (ETM+) instrument onboard the spacecraft.

177 *2.3 Albedo and moisture data*

178 Broadband shortwave albedo (Figure 2G-I) and the Land Surface Water Index (LSWI; Figure
179 2D-F) were estimated from the narrowband surface reflectance layers of the Landsat 7 Level 2
180 Collection 2 Tier 1 Science Product acquired for the same dates and times as the surface
181 temperature data. Surface reflectance data was atmospherically corrected using the Landsat

Ecosystem Disturbance Adaptive Processing System (LEDAPS) which generates surface reflectance estimates from a radiative transfer model with inputs of TOA reflectance, TOA brightness temperature, and auxiliary data such as water vapor, ozone, geopotential height, aerosol optical depth, and digital elevation (Masek et al. 2006). Albedo was estimated using the narrowband to broadband shortwave albedo algorithm developed for the ETM+ instrument in Liang (2001) and validated in Liang et al. (2003). Surface albedo was estimated as:

$$\alpha_{ETM+} = 0.356\alpha_1 + 0.130\alpha_3 + 0.373\alpha_4 + 0.085\alpha_5 + 0.072\alpha_7 - 0.0018 \quad (1)$$

where α_{ETM+} is the estimated broadband shortwave surface albedo and α_1, α_3, α_4, α_5, and α_7 correspond to the atmospherically-corrected surface reflectance within spectral bands 1 (blue), 3 (red), 4 (near-infrared), 5 (short-wave infrared), and 7 (mid-infrared) of the ETM+ instrument. Albedo was estimated for all clear sky pixels in Landsat 7 images collected during JJA of the five years prior to the year depicted by each city's landcover map and composited to create a raster of mean JJA clear sky surface albedo during the sunlit Landsat overpass time across each city.

We use LSWI to characterize the moisture content of vegetation as a proxy for potential latent heat flux, as vegetation in water scarce environments likely transpires less than vegetation with sufficient access to water. LSWI (sometimes referred to as the Land Surface Moisture Index or Normalized Difference Water Index; Ji et al. 2011) has been demonstrated to be effective in monitoring vegetation moisture content (Maki et al. 2004; Gu et al. 2008) and was estimated as:

$$LSWI = \frac{\alpha_4 - \alpha_5}{\alpha_4 + \alpha_5} \quad (2)$$

where composites were produced in the same way as the surface temperature and albedo rasters.

2.4 Census block boundaries

Census block geographic boundaries were extracted for each city from the Topologically Integrated Geographic Encoding and Referencing Database (TIGER; U.S. Census Bureau 2019a).

Census blocks represent the smallest geographic area for which the U.S. Census Bureau collects data and are defined as "statistical areas bounded on all sides by visible features, such as streets, roads, streams, and railroad tracks, and/or by nonvisible boundaries such as city, town, township, and county limits, and short line-of-sight extensions of streets and roads" (U.S. Census Bureau 2019b). Census blocks were chosen as the unit of aggregation and analysis for the gridded landcover, surface temperature, LSWI, and albedo data as they are meaningful units for the scale of typical (re)development and land use planning projects taken on by cities and so that data from this analysis can be coupled to other census geographies for pairing with sociodemographic data collected by the U.S. Census Bureau for future analysis (SI Table 2; SI Figure 2). For each city, landcover data was aggregated to the census block level by computing the percent of each landcover type within each census block. Surface temperature, LSWI, and albedo data were aggregated to the census block level by computing the mean values of all pixels with a pixel centroid falling within a census block. Census blocks less than 3600 m^2 in area were omitted from the analysis as they are smaller than the native spatial resolution of the Landsat 7 infrared thermal bands used in the derivation of the surface temperature data product used in this analysis. The minimum area requirement removed an average of 4.7% of census blocks per city from the analysis, ranging from 1.1% of census blocks in Durham, up to 10.0% of census blocks in Boston (SI Table 2). As this analysis focuses on white roof and greenspace impacts on surface temperature across developed landscapes, census blocks with less than 1% building cover were also omitted from the analysis.

2.5 Spatial regression modeling - Spatial Durbin Error Model

To estimate the impact of land cover composition and albedo on surface temperature at the census block level for each city, we implement a Spatial Durbin Error Model (SDEM; LeSage &

228 Pace 2009), which includes spatial lag effects on the independent variables and model error to
229 estimate direct and indirect impacts of independent variables on the dependent variable at the
230 census block level. We utilize a spatial autoregressive framework due to spatial autocorrelation in
231 the temperature data, which may bias the coefficient estimates from a traditional ordinary least
232 squares regression modeling framework (Lichstein et al. 2002). The SDEM form is:

233 $$y = X\beta + WX\theta + u, \quad (3)$$

234 $$u = \lambda Wu + \varepsilon,$$

235 $$\varepsilon \sim N(0, \sigma^2)$$

236 where y is the dependent variable vector (mean surface temperature (K)), X is the independent
237 variable matrix (tree cover (%), grass cover (%), building cover (%), other paved surface cover
238 (%), and mean albedo (unitless)), β is the regression parameter vector, W is a spatial weighting
239 matrix, θ is the independent spatial lag parameter vector, u is the spatial error, λ is the spatial
240 coefficient of the error, and ε is the error vector of the model. In the San Jose SDEM, grass was
241 disaggregated in the independent variable matrix into irrigated versus non-irrigated grass cover.
242 The spatial weighting matrix, W, was constructed using the variance-stabilizing 'S-coding'
243 scheme described by Tiefelsdorf et al. (1999) to reduce heterogeneity in spatial weights due to
244 differences in the number and size of neighbors. Direct impacts, represented by β, describe the
245 impact of a unit change in the independent variable within a focal unit (in this analysis, within a
246 census block) on the dependent variable. Indirect impacts, represented by θ, capture spatial
247 spillover effects and describe the effect of a unit change in the independent variable within the
248 spatially weighted neighboring observations on the dependent variable of the focal unit.

249 Bare land cover and road cover were omitted from the SDEMs of all cities to minimize
250 multicollinearity. We computed the variance inflation factor (VIF) for each independent variable

within each city-specific SDEM to evaluate the extent to which SDEM impact coefficient estimates are driven by multicollinearity. We find 31 out of 36 VIFs to be less than five and all VIFs to be less than ten (SI Table 3), indicating that multicollinearity is not a concern (Kennedy 2018). To test for spatial autocorrelation of SDEM residuals in each city, we conducted a two-sided Moran's I test on the error of the SDEM finding no evidence of spatial autocorrelation in the error (SI Table 4). Model validation was conducted for the SDEM of each city by randomly selecting 70% of census blocks within each city to use as a training dataset, and predicting the mean surface temperature in a testing dataset composed of the remaining 30% of census blocks as a function of land cover composition and albedo.

2.6 Sensitivity analysis of greenspace impact drivers

We test the sensitivity of the magnitude of grass cover and tree cover cooling impacts to vegetation moisture availability and solar irradiance - two environmental drivers that impose limits on evapotranspirative cooling (Jarvis & McNaughton 1986) - using two ordinary least squares regression analyses. For tree cover cooling impacts, we fit a linear model of the form:

$$\beta_{SDEM,tree} = \alpha + \beta_1 \times GHI_{JJA} + \beta_2 \times LSWI_{tree} + \varepsilon \quad (4)$$

where $\beta_{SDEM,tree}$ is the tree cover direct impact (K $\%^{-1}$) estimated by the SDEM of each city, α is the model intercept, β_1 is the sensitivity of $\beta_{SDEM,tree}$ to GHI_{JJA}, β_2 is the sensitivity of $\beta_{SDEM,tree}$ to $LSWI_{tree}$, GHI_{JJA} is the mean daytime JJA clear sky global horizontal irradiance for each city (W m^{-2}; obtained for the years 2019 - 2020 from the National Solar Radiation Database, 2022), $LSWI_{tree}$ is the mean LSWI of all 30-meter x 30-meter Landsat pixels that contain more than 25% tree cover (unitless), and ε is the model error. Significant model coefficients of a similar magnitude were observed across pixel tree cover thresholds ranging from 5% to 95%. We choose 25% as the

threshold for tree and grass cover in the sensitivity analysis as it restricts the analysis to only include pixels where tree or grass cover is a dominant land cover type.

For grass cover cooling impacts, we did not observe a significant relationship between $\beta_{SDEM,grass}$ and GHI_{JJA}. Therefore, we fit a linear model of the form:

$$\beta_{SDEM,grass} = \alpha + \beta \times LSWI_{grass} + \varepsilon \quad (5)$$

where $\beta_{SDEM,grass}$ is the grass cover direct impact (K %$^{-1}$) estimated by the SDEM of each city, α is the model intercept, β is the sensitivity of $\beta_{SDEM,grass}$ to $LSWI_{grass}$, $LSWI_{grass}$ is the mean LSWI of all 30-meter x 30-meter Landsat pixels that contain more than 25% grass cover (unitless), and ε is the model error. All modeling and statistical testing were conducted using R version 4.1 (R Core Team 2022).

3. Results

3.1 Model evaluation and validation

We find strong agreement between the observed versus predicted surface temperature estimates (Figure 3). The SDEMs capture much of the variance in surface temperature with out-of-sample R^2 values ranging from 0.51 in the San Jose SDEM to 0.89 in the Charlotte SDEM (Figure 3). We find no evidence of substantial bias in SDEM predictions of surface temperature with all regression slopes close to one (range of 0.97 - 1.07) and intercepts close to zero (range of -30.15 - 8.58). Further, we find evidence of strong predictive power across all city-specific SDEMs with an average out-of-sample root mean square error of 1.36 K across all cities, which is equal to just 6.0% of the range of observed surface temperature values across all cities (300.97 K – 323.62 K; Figure 3).

3.2 Impact estimates

295 The direct impact coefficients were highly significant ($p < 0.001$) across all cities for each
296 independent variable included in the SDEMs (Figure 4A; Table 2). Tree cover had a negative
297 (cooling) direct impact on surface temperature in each city, ranging from -0.051 K $\%^{-1}$ in Chicago
298 to -0.123 K $\%^{-1}$ in Durham. Grass cover had a negative direct impact in all cities except for San
299 Jose, where irrigated grass cover was distinguished from non-irrigated grass cover. We found a
300 positive (warming) direct impact of non-irrigated grass cover of 0.022 K $\%^{-1}$ in San Jose versus a
301 negative direct impact of irrigated grass cover of -0.018 K $\%^{-1}$, suggesting that irrigated grass cover
302 has a stronger cooling impact than non-irrigated grass cover in arid cities. The mean direct impact
303 of tree cover on surface temperature (-0.089 K $\%^{-1}$) was approximately four times stronger than
304 the mean direct impact of grass cover (-0.021 K $\%^{-1}$), providing evidence that urban surface
305 temperatures are more sensitive to tree cover than grass cover (Figure 4A) during the daytime. We
306 estimate significant spatial spillover effects of tree cover, where indirect impacts describe the
307 effect of a unit change in tree cover within the spatially weighted neighboring observations on the
308 surface temperature of a focal census block, with negative indirect impacts of tree cover observed
309 across all seven cities (Figure 4B) with a mean indirect impact of -0.047 K $\%^{-1}$. In contrast,
310 significant negative indirect impacts of grass cover were only observed in three cities and were
311 more than 90% weaker than the indirect impacts of tree cover with an average indirect impact of
312 just -0.004 K $\%^{-1}$ (Table 2; Figure 4B).
313 Both building cover and other paved cover had significant positive direct impacts on
314 surface temperature, however, the positive impacts of building cover and other paved cover were
315 weaker than the negative impact of tree cover in each city. Additionally, we found less variability
316 in the building cover and other paved cover direct impacts (σ = 0.014 K $\%^{-1}$ and 0.007 K $\%^{-1}$,
317 respectively) than grass cover (σ = 0.024 K $\%^{-1}$) and tree cover (σ = 0.024 K $\%^{-1}$) direct impacts.

We find solar irradiance and vegetation moisture content to be strong controls on the magnitude of tree cover direct impacts.

Mean JJA global horizontal solar irradiance and the mean LSWI of Landsat pixels containing more than 25% tree cover explain 97% of the variance in tree cover direct impacts (Figure 5A), suggesting that the magnitude of tree cover cooling impacts is a function of solar radiation intensity and vegetation moisture availability. We observe the strongest direct grass cover impacts in the cities with the highest vegetation moisture content, with the mean LSWI of Landsat pixels containing more than 25% grass cover explaining 89% of the variance in grass cover direct impacts (Figure 5B), highlighting that the sensitivity of surface temperature to grass cover is largely a function of moisture availability.

Albedo was found to impose a strong negative direct impact on surface temperature of a similar magnitude across all cities (Figure 4A) with an average direct impact of -0.187 K per albedo increase of 0.01 (unitless). Furthermore, albedo was found to impose significant, but weaker, indirect effects (Figure 4B) on surface temperature in six out of seven cities with an average indirect impact of -0.085 K per albedo increase of 0.01. The marginal impacts of tree cover and albedo estimated here support both urban greening and integration of high albedo surfaces as effective ways to reduce surface temperatures, however, we find large discrepancies in the range of typical observed values of albedo versus tree cover within and across cities (Figure 6). Tree cover values were more variable than albedo values with a coefficient of variation of tree cover at the census block level of 0.69 compared to a coefficient of variation of albedo at the census block level of 0.13.

4. Discussion

4.1 Urban greenspace impacts on surface temperature

While we have long known that vegetation and albedo impact temperature, this study advances our understanding of the marginal cooling impacts of urban green space and albedo across developed landscapes that vary in land cover composition and background climate. We identify significant differences in both the cooling efficiency of tree versus grass cover and the cooling efficiency of irrigated versus non-irrigated grass cover in an arid city. Furthermore, we leverage differences in vegetation moisture content and mean solar irradiance to gain insights into the drivers of vegetation cooling potential within and across cities. We expand upon existing studies of urban vegetation cooling efficiency that primarily focus on trees or vegetation as a whole by separating grass effects from tree effects. Grass cover comprises up to 24.8% of land area in the cities investigated here, and is more abundant than tree cover in three of the seven cities investigated here (Figure 1), pointing to the importance of understanding the cooling effects from each vegetation type.

The magnitude of marginal cooling impacts of vegetation reported here (mean of -0.089 K $\%^{-1}$ and -0.021 K $\%^{-1}$ for tree and grass cover, respectively) is consistent with previous studies. In a literature review conducted by Wang et al. (2020), reported urban vegetation cooling efficiency values range from -0.029 K $\%^{-1}$ to -0.318 K $\%^{-1}$ with an average value of -0.081 K $\%^{-1}$. Wang et al. (2020) found the marginal cooling impacts of tree cover across 118 United States cities to range from -0.040 K $\%^{-1}$ to -0.574 K $\%^{-1}$ but did not quantify grass cover cooling impacts. While this study quantifies the marginal cooling impacts of vegetation during mean JJA daytime conditions, there is evidence that the sensitivity of land surface temperature to vegetation cover increases during heat waves. Wang et al. (2019) found stronger average marginal cooling impacts (-0.202 K $\%^{-1}$) than those observed in this study during heat waves in six United States cities, along with a significant relationship between mean land surface temperature and marginal cooling impact,

highlighting the potential for heat mitigation from urban greening strategies under projected future increases in extreme heat.

The SDEM results reported here corroborate the notion that incorporating vegetation into developed landscapes can reduce surface temperatures, however, different mechanisms of cooling between tree cover and grass cover result in a stronger local cooling impact of tree cover than grass cover with a stronger cooling spillover, indirect impact of trees on the surrounding area. Trees cool the surface via shading (Yu et al. 2020) and evapotranspiration (Rahman et al. 2017), whereas grass primarily cools the surface via evapotranspiration. Therefore, when evapotranspiration efficiency is constrained by moisture availability, the cooling potential of grassy surfaces is expected to decline while the primary cooling mechanism of tree cover is expected to shift towards shading. At the 60 m native spatial resolution of the Landsat 7 infrared thermal bands used in this analysis, it is unlikely that the stronger cooling impacts of tree cover versus grass cover observed here are resultant from shade effects alone. Instead, it is possible that the stronger tree cover cooling impacts are a function of increased evapotranspiration associated with the high leaf area index and increased exposure to the sun and sky of broadleaf trees prevalent in cities (Pataki et al. 2011) compared to shorter statured grasses and shrubs. The impact coefficients and relationship between tree cover direct impacts, solar irradiance, and moisture availability (Figure 5A) reported here imply that tree canopy expansion is likely a more effective climate adaptation strategy in cities at a lower latitude with adequate precipitation or irrigation to sustain evapotranspiration. Despite variability in the magnitude of tree cover impacts observed across cities, we find evidence of tree cover expansion as an effective heat mitigation strategy across all cities included in the analysis.

386 In considering regions to implement canopy expansion measures within cities, the strongest
387 cooling impacts may be realized in neighborhoods with a higher fraction of impervious surface
388 area, with adequate space for canopy expansion, due to the thermal properties and moisture
389 availability of the surfaces underlying the canopy (Rahman et al. 2020). Our results suggest that
390 canopy expansion over paved surfaces has a larger impact than canopy expansion over grassy
391 surfaces due to the compounded effect of reduced surface temperatures from each additional
392 fraction of canopy plus surface temperature reductions resultant from decreased pavement area.
393 The thermal admittance of anthropogenic construction materials with a low water holding capacity
394 typically found below highly urbanized canopies (e.g. asphalt, concrete, and brick) is often lower
395 than that of saturated natural materials than can readily store water (Oke 1987; Thornes and Shao
396 1991; Crevier and Delage 2001). Materials with a lower thermal admittance are characterized by
397 a lower heat storage capacity and therefore shed large amounts of sensible heat, resulting in high
398 daytime surface temperatures. Rahman et al. (2019) demonstrate the influence of surfaces
399 underlying tree canopies, finding that in Munich, Germany, a unit increase in the leaf area index
400 of trees above the surface results in a 3 K decrease in the surface temperature of grassy surfaces
401 compared to a 6 K decrease in the surface temperature of asphalt. Critically, the existing land cover
402 composition represents an important consideration in climate-sensitive design strategies that focus
403 on urban greening.

404 In addition to land cover composition, we find a strong influence of the regional moisture
405 regime on the cooling potential of grass cover. Arid cities that lack a reliable supply of water via
406 precipitation during the summer months, such as San Jose and San Diego (Table 1), require
407 irrigation to realize the cooling effects of grass cover which can strain local water supplies. In the
408 southwestern United States, more than one-third of regional water supplies can be used to irrigate

409 urban landscapes (Devitt et al. 2008). In cities located in dry climates, urban greening strategies
410 that focus on tree canopy expansion are likely to reduce heat exposure more than strategies that
411 treat all vegetation, including grass, as equal, while simultaneously reducing water consumption.
412 Wynne and Devitt (2020) found that in the arid climate of Las Vegas, Nevada, irrigated tree-
413 dominated landscapes had lower water use rates than similar areas dominated by irrigated
414 turfgrass. In contrast, cities located in mesic climates with a consistent supply of precipitation
415 during the summer months can achieve considerable surface temperature reductions from grass
416 cover alone. For example, we find the direct impact of grass cover in the mesic city of Boston (-
417 0.058 K $\%^{-1}$) to be 73% of the direct impact of tree cover in Boston (-0.079 K $\%^{-1}$; Table 2),
418 whereas the direct impact of grass cover in San Diego (-0.007 K $\%^{-1}$) is only 7.4% of the direct
419 impact of tree cover (-0.094 K $\%^{-1}$; Table 2). These findings point to the importance of moving
420 beyond simple greenness indices, such as NDVI, that are commonly used to characterize urban
421 greenspace, towards metrics that better capture the form and function of urban vegetation and
422 associated differences in ecosystem service provisions.

423 *4.2 Trade-offs of urban greening and albedo manipulation*

424 This analysis points to both urban greening and the incorporation of high albedo surfaces as
425 effective ways to combat high surface temperatures. Efforts to improve heat resiliency through
426 climate sensitive design should consider the trade-offs of potential adaptation strategies. Rooftops
427 are a common target for the installation of reflective surfaces and account for up to 25% of the
428 total landcover in the seven cities investigated here (Figure 1), with buildings accounting for more
429 area than tree canopy in Chicago, San Diego, and San Jose, highlighting the adoption of white
430 roofs as a potentially high impact intervention for improved thermal comfort via albedo increases.
431 White roof adoption offers a low-cost, easy to implement, heat mitigation option with long-term

net savings compared to traditional dark roofs (Sproul et al. 2014). Moreover, white roofs offer additional environmental benefits via energy savings and reduced greenhouse gas emissions associated with reduced cooling demand during the summer months (Giordano et al. 2019). The cooling services associated with white roofs are realized immediately following implementation, but deteriorate over time as pollutants and dirt accumulate on the roof surface (Figure 7). An average decrease in rooftop albedo of 0.15 may be expected within the first year of white roof adoption, with a continued gradual decline in subsequent years (Bretz & Akbari 1997).

In contrast, the financial cost (Vogt et al. 2015) and greenhouse gas emissions associated with the planting, irrigation, maintenance, and disposal of city trees can be high (Kendall and McPherson 2011) and require trees to survive for several decades to attain carbon neutrality (Petri et al. 2016). However, while cool pavements/white roofs singularly benefit public health via thermal regulation, urban vegetation has been demonstrated to provide a suite of co-benefits to public health and well-being (Markevych et al. 2017). Urban greenspace decreases exposure to other environmental stressors such as noise (van Renterghem et al. 2015) and air pollution (Escobedo et al. 2011), reduces psychophysiological stress (Hartig et al. 2014), encourages physical activity (Almanza et al. 2012), and facilitates social cohesion (Weinstein et al. 2015). Over time, the ecosystem services associated with urban greening are enhanced as larger trees cast more shade and transpire more water than smaller trees (Figure 7).

4.3 Potential public health applications

Surface temperature observations offer several advantages over air temperature observations in assessing the urban thermal condition. Air temperature observations are commonly made at relatively few discrete locations with multiple sensors across a city or are estimated via a coarse resolution gridded reanalysis product. In contrast, remote sensing measurements of surface

455 temperature offer long-term, high-resolution observations using the same sensor with global
456 coverage. Thus, surface temperature can expand opportunities to identify localized modifiable
457 drivers of heat exposure (e.g., vegetation and albedo), and characterize fine scale heat exposure
458 disparities and associated health risks. Limitations of surface temperature observations include
459 uncertainty due to cloud cover, trade-offs between spatial and temporal resolution, and
460 discrepancies between surface and air temperature (Zhou et al. 2018), where air temperature is
461 more closely related to public health than surface temperature. Currently the health effects
462 literature is primarily based on measured or perceived air temperature (Anderson et al. 2013), with
463 limited studies linking surface temperature to health (Smargiassi et al. 2009, Kestens et al. 2011).
464 Surface temperature is largely a function of the incoming solar energy, moisture availability,
465 and thermal properties of the surface material. The air temperature felt by humans, however,
466 experiences temperature change via the convective transport of sensible heat from surrounding
467 surfaces, net radiation changes where urban pollutants, aerosols, and humidity absorb and emit
468 energy, and advection of heat from adjacent air parcels. Thus, the surface temperature imposes a
469 strong control on air temperature, but the dependence of air temperature on other factors such as
470 wind speed, aerodynamic roughness, and the temperature of large-scale air masses precludes the
471 simple prediction of air temperature from surface temperature alone (Venter et al. 2021).
472 Surface temperature observations may also be informative for identifying neighborhoods
473 susceptible to prolonged exposure events that persist overnight as the thermal emissions of the
474 surface become a primary driver of air temperature at night (Ibsen et al. 2022) when solar radiation
475 inputs cease and turbulent mixing subsides. Extended periods of heat exposure exacerbate
476 physiological stress on the human body and can increase the risk of negative heat-related health
477 outcomes (WHO 2018). The City of Boston (2022) reports that in neighborhoods with the highest

478 average surface temperature, the associated air temperature can remain over 32 °C overnight
479 during heat waves, with daytime air temperatures reaching up to 41 °C.

480 Marginalized communities tend to experience more heat exposure than other communities in
481 warm countries (Park et al. 2015) highlighting a critical need to target disproportionalities in heat
482 exposure observed across communities in the deployment of climate-sensitive infrastructure. Hsu
483 et al. (2021) find that at the census tract level in the United States, the average person of color is
484 exposed to warmer surface temperatures than non-Hispanic white populations in 97% of the 175
485 largest urbanized areas in the country, with similar relationships observed when comparing
486 households below the US Census Bureau's poverty threshold to those at more than twice the
487 poverty threshold. Tieskens et al. (2022) find substantial spatial variability in residential demand
488 for cooling as a function of heat exposure and population characteristics at the census tract level
489 in Boston, MA, pointing to the importance of spatially comprehensive assessment of cooling
490 strategies. We choose to conduct our analysis at the census block level to accommodate
491 aggregation of temperature, land cover, and albedo data to the census block group or census tract
492 level for future pairing with sociodemographics and health in studies of exposure disparities and
493 vulnerability.

494 Overall, the methods described in this paper facilitate modeling of land surface temperature
495 changes due to fine scale vegetation and albedo interventions, providing the opportunity to
496 evaluate the impact of these interventions on exposure disparities and health studies in future
497 projects.

498 *4.4 Winter impacts*

499 The cooling impacts reported here describe temperature reductions observed during summer
500 months. Much less attention has been given to the wintertime urban heat island effect, but the

implementation of climate sensitive urban design choices may produce unforeseen consequences during colder periods in temperate climates. The wintertime urban heat island effect has been shown to potentially reduce cold-related mortality by up to 15% (Macintyre et al. 2021a). Deciduous trees that lose their leaves in the winter allow for solar radiation to penetrate the canopy and reach the surface, resulting in warmer wintertime temperatures. White roofs continue to reflect wintertime radiation away from the surface, resulting in lower wintertime temperatures (He et al. 2020a), increased building heating costs at higher latitudes (Oleson et al. 2010), and uncertain impacts on wintertime mortality. Macintyre et al (2021b) project that the summertime health benefits of white roofs will increase throughout the 21st century in the United Kingdom, with insignificant changes in the impact of white roofs on cold-related mortality. In contrast, He et al. (2020b) estimate that in the Greater Boston area, 0.21% of deaths attributed to summertime heat exposure may be avoided through the implementation of white roofs, compared to 0.096% of wintertime deaths associated with exposure to extreme cold temperatures attributed to cool roof impacts on wintertime temperatures.

5. Conclusion

We estimate strong, significant cooling impacts of tree cover and albedo on surface temperatures at the census block scale across seven United States cities. We find tree cover cooling impacts increase at lower latitudes and in more mesic climates. We find evidence of grass as a cooling mechanism with a smaller impact than tree cover that is largely controlled by moisture availability. The impact coefficients and drivers identified here offer valuable information to city planners working to incorporate the most effective climate sensitive design strategies that promote heat resiliency given the current land cover composition and background climate. For example, in arid cities with low latent heat flux efficiency and a reduced capacity to maintain healthy

vegetation without irrigation, cool roofs and cool pavements offer a way to cool the city surface without consuming excess water resources. Conversely, in mesic temperate climates with ample precipitation, cities would likely benefit from the incorporation of both urban greening and white roof adoption, where tree cover benefits may be more impactful in neighborhoods characterized by high impervious surface fractions.

Acknowledgements

Financial support for this research was provided by National Science Foundation awards DGE-1840990, ICER-1854706, and DGE-1735087. We thank Professor Dan Li for helpful comments on the analysis and the Boston University Master of Science in Statistical Practice Consulting group for assistance in statistical methodology.

References

Almanza, E., Jerrett, M., Dunton, G., Seto, E., & Ann Pentz, M. (2012). A study of community design, Greenness, and physical activity in children using satellite, GPS and Accelerometer Data. *Health & Place*, *18*(1), 46–54. https://doi.org/10.1016/j.healthplace.2011.09.003

Anderson, G. B., Bell, M. L., & Peng, R. D. (2013). Methods to calculate the heat index as an exposure metric in environmental health research. *Environmental Health Perspectives*, *121*(10), 1111–1119. https://doi.org/10.1289/ehp.1206273

Bekkar, B., Pacheco, S., Basu, R., & DeNicola, N. (2020). Association of air pollution and heat exposure with preterm birth, low birth weight, and stillbirth in the US. *JAMA Network Open*, *3*(6). https://doi.org/10.1001/jamanetworkopen.2020.8243

Bell, J.E., S.C. Herring, L. Jantarasami, C. Adrianopoli, K. Benedict, K. Conlon, V. Escobar, J. Hess, J. Luvall, C.P. Garcia-Pando, D. Quattrochi, J. Runkle, and C.J. Schreck, III, 2016: Ch. 4: Impacts of Extreme Events on Human Health. *The Impacts of Climate Change on Human Health in the United States: A Scientific Assessment*. U.S. Global Change Research Program, Washington, DC, 99–128. http://dx.doi.org/10.7930/J0BZ63ZV

Bretz, S. E., & Akbari, H. (1997). Long-term performance of high-albedo roof coatings. *Energy and Buildings*, *25*(2), 159–167. https://doi.org/10.1016/s0378-7788(96)01005-5

Carlson, T. N., & Boland, F. E. (1978). Analysis of urban-rural canopy using a surface heat flux/temperature model. *Journal of Applied Meteorology*, *17*(7), 998–1013. https://doi.org/10.1175/1520-0450(1978)017<0998:aourcu>2.0.co;2

Crevier, L.P., & Delage, Y. (2001). Metro: A new model for road-condition forecasting in Canada. *Journal of Applied Meteorology*, *40*(11), 2026–2037. https://doi.org/10.1175/1520-0450(2001)040<2026:manmfr>2.0.co;2

Devitt, D. A., Carstensen, K., & Morris, R. L. (2008). Residential Water Savings associated with satellite-based et irrigation controllers. *Journal of Irrigation and Drainage Engineering*, *134*(1), 74–82. https://doi.org/10.1061/(asce)0733-9437(2008)134:1(74)

Easterling, D., Kunkel, K., Lewis, K., Reidmiller, D., Stewart, B., Eds., *Impacts, Risks, and Adaptation in the United States: Fourth National Climate Assessment, Volume II: Report-in-Brief* (U.S. Global Change Research Program, 2018); 10.7930/NCA4.2018.RiBGraff

Environmental Protection Agency. (April 2021). *Climate Change Indicators: Heat-Related Deaths*. EPA. Retrieved June 5, 2022, from https://www.epa.gov/climate-indicators/climate-change-indicators-heat-related-deaths

Erell, E., Pearlmutter, D., Boneh, D., & Kutiel, P. B. (2014). Effect of high-albedo materials on pedestrian heat stress in Urban Street Canyons. *Urban Climate*, *10*, 367–386. https://doi.org/10.1016/j.uclim.2013.10.005

Escobedo, F. J., Kroeger, T., & Wagner, J. E. (2011). Urban forests and pollution mitigation: Analyzing Ecosystem Services and disservices. *Environmental Pollution*, *159*(8-9), 2078–2087. https://doi.org/10.1016/j.envpol.2011.01.010

Giordano, F., Tulumen, Z., Sanchez, R., & Magnacca, G. (2019). White roof as multiple benefits low-cost technology. *CERN IdeaDquare Journal of Experimental Innovation, 3*(2), *12-17*. https://doi.org/10.23726/cij.2019.874

Gorelick, N., Hancher, M., Dixon, M., Ilyushchenko, S., Thau, D., & Moore, R. (2017). Google Earth Engine: Planetary-scale geospatial analysis for everyone. *Remote Sensing of Environment*, *202*, 18–27. https://doi.org/10.1016/j.rse.2017.06.031

Grimm, N. B., Faeth, S. H., Golubiewski, N. E., Redman, C. L., Wu, J., Bai, X., & Briggs, J. M. (2008). Global change and the ecology of Cities. *Science*, *319*(5864), 756–760. https://doi.org/10.1126/science.1150195

Gu, Y., Hunt, E., Wardlow, B., Basara, J. B., Brown, J. F., & Verdin, J. P. (2008). Evaluation of MODIS NDVI and NDWI for vegetation drought monitoring using Oklahoma mesonet soil moisture data. *Geophysical Research Letters*, *35*(22). https://doi.org/10.1029/2008gl035772

Hartig, T., Mitchell, R., de Vries, S., & Frumkin, H. (2014). Nature and health. *Annual Review of Public Health*, *35*(1), 207–228. https://doi.org/10.1146/annurev-publhealth-032013-182443

Heal, G., & Park, J. (2016). Reflections—temperature stress and the direct impact of climate change: A review of an emerging literature. *Review of Environmental Economics and Policy*, *10*(2), 347–362. https://doi.org/10.1093/reep/rew007

He, C., Zhao, J., Zhang, Y., He, L., Yao, Y., Ma, W., & Kinney, P. L. (2020a). Cool roof and green roof adoption in a metropolitan area: Climate impacts during summer and Winter.

593 *Environmental Science & Technology*, *54*(17), 10831–10839.
594 https://doi.org/10.1021/acs.est.0c03536

595 He, C., He, L., Zhang, Y., Kinney, P. L., & Ma, W. (2020b). Potential impacts of cool and green
596 roofs on temperature-related mortality in the Greater Boston Region. *Environmental*
597 *Research Letters*, *15*(9), 094042. https://doi.org/10.1088/1748-9326/aba4c9

598 Hsu, A., Sheriff, G., Chakraborty, T., & Manya, D. (2021). Disproportionate exposure to urban
599 heat island intensity across major US cities. *Nature Communications*, *12*(1).
600 https://doi.org/10.1038/s41467-021-22799-5

601 Ibsen, P. C., Jenerette, G. D., Dell, T., Bagstad, K. J., & Diffendorfer, J. E. (2022). Urban
602 landcover differentially drives day and nighttime air temperature across a semi-arid city.
603 *Science of The Total Environment*, *829*, 154589.
604 https://doi.org/10.1016/j.scitotenv.2022.154589

605 IPCC, 2021: Climate Change 2021: The Physical Science Basis. Contribution of Working Group
606 I to the Sixth Assessment Report of the Intergovernmental Panel on Climate Change
607 [Masson-Delmotte, V., P. Zhai, A. Pirani, S.L. Connors, C. Péan, S. Berger, N. Caud, Y.
608 Chen, L. Goldfarb, M.I. Gomis, M. Huang, K. Leitzell, E. Lonnoy, J.B.R. Matthews,
609 T.K. Maycock, T. Waterfield, O. Yelekçi, R. Yu, and B. Zhou (eds.)]. Cambridge
610 University Press. In Press.

611 Ji, L., Zhang, L., Wylie, B. K., & Rover, J. (2011). On the terminology of the spectral vegetation
612 index (NIR − swir)/(nir + SWIR). *International Journal of Remote Sensing*, *32*(21), 6901–
613 6909. https://doi.org/10.1080/01431161.2010.510811

614 Kendall, A., & McPherson, E. G. (2011). A life cycle greenhouse gas inventory of a tree
615 production system. *The International Journal of Life Cycle Assessment*, *17*(4), 444–452.
616 https://doi.org/10.1007/s11367-011-0339-x

617 Kennedy, P. (2018). *A guide to econometrics*. Wiley Blackwell.

618 Kestens, Y., Brand, A., Fournier, M., Goudreau, S., Kosatsky, T., Maloley, M., & Smargiassi, A.
619 (2011). Modelling the variation of land surface temperature as determinant of risk of heat-
620 related health events. *International Journal of Health Geographics*, *10*(1), 7.
621 https://doi.org/10.1186/1476-072x-10-7

622 Laraby, K. G., & Schott, J. R. (2018). Uncertainty estimation method and landsat 7 global
623 validation for the landsat surface temperature product. *Remote Sensing of Environment*,
624 *216*, 472–481. https://doi.org/10.1016/j.rse.2018.06.026

625 Jarvis, P. G., & McNaughton, K. G. (1986). Stomatal control of transpiration: Scaling up from
626 leaf to Region. *Advances in Ecological Research*, 1–49. https://doi.org/10.1016/s0065-
627 2504(08)60119-1

628 Leal Filho, W., Echevarria Icaza, L., Emanche, V., & Quasem Al-Amin, A. (2017). An evidence-
629 based review of impacts, strategies and tools to mitigate urban heat islands. *International*
630 *Journal of Environmental Research and Public Health*, *14*(12), 1600.
631 https://doi.org/10.3390/ijerph14121600

632 LeSage, J. P., & Pace, R. K. (2009). *Introduction to spatial econometrics*. CRC Press.

633 Li, D., Bou-Zeid, E., & Oppenheimer, M. (2014). The effectiveness of cool and green roofs as
634 urban heat island mitigation strategies. *Environmental Research Letters*, *9*(5), 055002.
635 https://doi.org/10.1088/1748-9326/9/5/055002

636 Li, D., Liao, W., Rigden, A. J., Liu, X., Wang, D., Malyshev, S., & Shevliakova, E. (2019).
637 Urban heat island: Aerodynamics or imperviousness? *Science Advances*, *5*(4).
638 https://doi.org/10.1126/sciadv.aau4299

639 Liang, S. (2001). Narrowband to broadband conversions of land surface albedo I. *Remote*
640 *Sensing of Environment*, *76*(2), 213–238. https://doi.org/10.1016/s0034-4257(00)00205-4

641 Liang, S., Shuey, C. J., Russ, A. L., Fang, H., Chen, M., Walthall, C. L., Daughtry, C. S. T., &
642 Hunt, R. (2003). Narrowband to broadband conversions of land surface albedo: II.
643 validation. *Remote Sensing of Environment*, *84*(1), 25–41. https://doi.org/10.1016/s0034-
644 4257(02)00068-8

645 Lichstein, J. W., Simons, T. R., Shriner, S. A., & Franzreb, K. E. (2002). Spatial autocorrelation
646 and autoregressive models in ecology. *Ecological Monographs*, *72*(3), 445–463.
647 https://doi.org/10.1890/0012-9615(2002)072[0445:saaami]2.0.co;2

648 Lynn, B. H., Carlson, T. N., Rosenzweig, C., Goldberg, R., Druyan, L., Cox, J., Gaffin, S.,
649 Parshall, L., & Civerolo, K. (2009). A modification to the NOAH LSM to simulate heat
650 mitigation strategies in the New York City metropolitan area. *Journal of Applied*
651 *Meteorology and Climatology*, *48*(2), 199–216. https://doi.org/10.1175/2008jamc1774.1

652 Macintyre, H. L., Heaviside, C., Cai, X., & Phalkey, R. (2021a). The Winter Urban Heat Island:
653 Impacts on cold-related mortality in a highly urbanized European region for present and
654 future climate. *Environment International*, *154*, 106530.
655 https://doi.org/10.1016/j.envint.2021.106530

656 Macintyre, H. L., Heaviside, C., Cai, X., & Phalkey, R. (2021b). Comparing temperature-related
657 mortality impacts of cool roofs in winter and summer in a highly urbanized European
658 region for present and future climate. *Environment International*, *154*, 106606.
659 https://doi.org/10.1016/j.envint.2021.106606

660 Maki, M., Ishiahra, M., & Tamura, M. (2004). Estimation of leaf water status to monitor the risk
661 of forest fires by using remotely sensed data. *Remote Sensing of Environment*, *90*(4), 441–
662 450. https://doi.org/10.1016/j.rse.2004.02.002

Markevych, I., Schoierer, J., Hartig, T., Chudnovsky, A., Hystad, P., Dzhambov, A. M., de Vries, S., Triguero-Mas, M., Brauer, M., Nieuwenhuijsen, M. J., Lupp, G., Richardson, E. A., Astell-Burt, T., Dimitrova, D., Feng, X., Sadeh, M., Standl, M., Heinrich, J., & Fuertes, E. (2017). Exploring pathways linking greenspace to health: Theoretical and methodological guidance. *Environmental Research*, *158*, 301–317. https://doi.org/10.1016/j.envres.2017.06.028

Masek, J. G., Vermote, E. F., Saleous, N. E., Wolfe, R., Hall, F. G., Huemmrich, K. F., Gao, F., Kutler, J., & Lim, T.-K. (2006). A landsat surface reflectance dataset for North America, 1990–2000. *IEEE Geoscience and Remote Sensing Letters*, *3*(1), 68–72. https://doi.org/10.1109/lgrs.2005.857030

Myint, S. W., Zheng, B., Talen, E., Fan, C., Kaplan, S., Middel, A., Smith, M., Huang, H.-ping, & Brazel, A. (2015). Does the spatial arrangement of urban landscape matter? examples of urban warming and cooling in Phoenix and Las Vegas. *Ecosystem Health and Sustainability*, *1*(4), 1–15. https://doi.org/10.1890/ehs14-0028.1

National Centers for Environmental Information. National Centers for Environmental Information, U.S. Climate Normals. [cited 2022 April 20]. Available from: https://www.ncei.noaa.gov/access/search/data-search/normals-annualseasonal-1991-2020

National Solar Radiation Database. [cited 2022 September 12]. Available from: https://nsrdb.nrel.gov/data-viewer

NYC CoolRoofs. NYC CoolRoofs - NYC Business. (n.d.). https://www1.nyc.gov/nycbusiness/article/nyc-coolroofs#report.

Oke, T. R. (1982). The energetic basis of the urban heat island. *Quarterly Journal of the Royal Meteorological Society*, *108*(455), 1–24. https://doi.org/10.1002/qj.49710845502

Oke, T. R. (1987). *Boundary layer climates*. Routledge.

Oke, T. R. (1988). The Urban Energy Balance. *Progress in Physical Geography: Earth and Environment*, *12*(4), 471–508. https://doi.org/10.1177/030913338801200401

Oke, T., Mills, G., Christen, A., and Voogt, J. (2017). *Urban Climates*. Cambridge: Cambridge University Press, doi: 10.1017/9781139016476

Oleson, K. W., Bonan, G. B., & Feddema, J. (2010). Effects of white roofs on urban temperature in a global climate model. *Geophysical Research Letters*, *37*(3). https://doi.org/10.1029/2009gl042194

Park, J., Hallegatte, S., Bangalore, M., & Sandhoefner, E. (2015). Households and heat stress: Estimating the distributional consequences of climate change. *Policy Research Working Papers*. https://doi.org/10.1596/1813-9450-7479

Park, R. J., Goodman, J., Hurwitz, M., & Smith, J. (2020). Heat and learning. *American Economic Journal: Economic Policy*, *12*(2), 306–339. https://doi.org/10.1257/pol.20180612

Pataki, D. E., McCarthy, H. R., Litvak, E., & Pincetl, S. (2011). Transpiration of urban forests in the Los Angeles Metropolitan Area. *Ecological Applications*, *21*(3), 661–677. https://doi.org/10.1890/09-1717.1

Petri, A. C., Koeser, A. K., Lovell, S. T., & Ingram, D. (2016). How green are trees? — using life cycle assessment methods to assess net environmental benefits. *Journal of Environmental Horticulture*, *34*(4), 101–110. https://doi.org/10.24266/0738-2898-34.4.101

R Core Team. (2022). *R: A Language and Environment for Statistical Computing*. Vienna: R Foundation for Statistical Computing.

Rahman, M. A., Moser, A., Rötzer, T., & Pauleit, S. (2017). Microclimatic differences and their influence on transpirational cooling of Tilia cordata in two contrasting street canyons in Munich, Germany. *Agricultural and Forest Meteorology*, *232*, 443–456. https://doi.org/10.1016/j.agrformet.2016.10.006

Rahman, M. A., Moser, A., Gold, A., Rötzer, T., & Pauleit, S. (2018). Vertical air temperature gradients under the shade of two contrasting urban tree species during different types of summer days. *Science of The Total Environment*, *633*, 100–111. https://doi.org/10.1016/j.scitotenv.2018.03.168

Rahman, M. A., Moser, A., Rötzer, T., & Pauleit, S. (2019). Comparing the transpirational and shading effects of two contrasting urban tree species. *Urban Ecosystems*, *22*(4), 683–697. https://doi.org/10.1007/s11252-019-00853-x

Rahman, M. A., Stratopoulos, L. M. F., Moser-Reischl, A., Zölch, T., Häberle, K.-H., Rötzer, T., Pretzsch, H., & Pauleit, S. (2020). Traits of trees for cooling urban heat islands: A meta-analysis. *Building and Environment*, *170*, 106606. https://doi.org/10.1016/j.buildenv.2019.106606

Sarofim, M.C., S. Saha, M.D. Hawkins, D.M. Mills, J. Hess, R. Horton, P. Kinney, J. Schwartz, and A. St. Juliana, 2016: Ch. 2: Temperature-Related Death and Illness. *The Impacts of Climate Change on Human Health in the United States: A Scientific Assessment*. U.S. Global Change Research Program, Washington, DC, 43–68. http://dx.doi.org/10.7930/J0MG7MDX

Shi, L., Chu, E., & Debats Garrison, J. (2018). Explaining progress in climate adaptation planning across 156 U.S. municipalities. *Planning for Climate Change*, 340–351. https://doi.org/10.4324/9781351201117-38

Smargiassi, A., Goldberg, M. S., Plante, C., Fournier, M., Baudouin, Y., & Kosatsky, T. (2009). Variation of daily warm season mortality as a function of micro-urban Heat Islands.

Journal of Epidemiology & Community Health, *63*(8), 659–664. https://doi.org/10.1136/jech.2008.078147

Smith, I. A., Winbourne, J. B., Tieskens, K. F., Jones, T. S., Bromley, F. L., Li, D., & Hutyra, L. R. (2021). A satellite-based model for estimating latent heat flux from urban vegetation. *Frontiers in Ecology and Evolution*, *9*. https://doi.org/10.3389/fevo.2021.695995

Sproul, J., Wan, M.P., Mandel, B.H., & Rosenfeld, A.H. (2014). Economic comparison of white, green, and black flat roofs in the United States. *Energy and Buildings, 71*, 20-27. https://doi.org/10.1016/j.enbuild.2013.11.058

Taha, H. (1997). Urban climates and heat islands: Albedo, evapotranspiration, and anthropogenic heat. *Energy and Buildings*, *25*(2), 99–103. https://doi.org/10.1016/s0378-7788(96)00999-1

Taleghani, M., Sailor, D., & Ban-Weiss, G. A. (2016). Micrometeorological simulations to predict the impacts of heat mitigation strategies on pedestrian thermal comfort in a Los Angeles neighborhood. *Environmental Research Letters*, *11*(2), 024003. https://doi.org/10.1088/1748-9326/11/2/024003

Thornes, J.E., & J. Shao, 1991: Spectral analysis and sensitivity tests for a numerical road surface temperature prediction model. *Meteorological Magazine*, 120, 117–124

Tiangco, M., Lagmay, A. M., & Argete, J. (2008). Aster-based study of the night-time urban heat island effect in Metro Manila. *International Journal of Remote Sensing*, *29*(10), 2799–2818. https://doi.org/10.1080/01431160701408360

Tiefelsdorf, M., Griffith, D. A., & Boots, B. (1999). A variance-stabilizing coding scheme for spatial link matrices. *Environment and Planning A: Economy and Space*, *31*(1), 165–180. https://doi.org/10.1068/a310165

Tieskens, K. F., Smith, I. A., Jimenez, R. B., Hutyra, L. R., & Fabian, M. P. (2022). Mapping the gaps between cooling benefits of urban greenspace and population heat vulnerability. *Science of The Total Environment*, *845*, 157283. https://doi.org/10.1016/j.scitotenv.2022.157283

TIGER/Line Shapefiles (machine readable data files) / prepared by the U.S. Census Bureau, 2019a

TIGER/Line Shapefiles Technical Documentation / prepared by the U.S. Census Bureau, 2019b

University of Vermont Spatial Analysis Laboratory. 2012. High resolution land cover for San Jose, CA (2011). Burlington, VT: University of Vermont Spatial Analysis Laboratory. https://gis.w3.uvm.edu/utc/Landcover/SanJose_2011.zip

University of Vermont Spatial Analysis Laboratory. 2013a. High resolution land cover for Mecklenburg County, NC (2012). Burlington, VT: University of Vermont Spatial Analysis Laboratory. https://gis.w3.uvm.edu/utc/Landcover/Mecklenburg_County.zip

University of Vermont Spatial Analysis Laboratory. 2013b. High resolution land cover for Washington DC (2011). Burlington, VT: University of Vermont Spatial Analysis Laboratory. https://gis.w3.uvm.edu/utc/Landcover/WashingtonDC_2011.zip

University of Vermont Spatial Analysis Laboratory. 2016. High resolution land cover for Chicago Region (2010). Burlington, VT: University of Vermont Spatial Analysis Laboratory. https://datahub.cmap.illinois.gov/dataset/high-resolution-land-cover-cook-county-2010

University of Vermont Spatial Analysis Laboratory. 2017a. High resolution land cover for San Diego, CA (2014). Burlington, VT: University of Vermont Spatial Analysis Laboratory. https://gis.w3.uvm.edu/utc/Landcover/SanDiego_2014.zip

University of Vermont Spatial Analysis Laboratory. 2017b. High resolution land cover for Durham, North Carolina (2015). Burlington, VT: University of Vermont Spatial Analysis Laboratory. https://gis.w3.uvm.edu/utc/Landcover/DurhamNC_2015.zip

University of Vermont Spatial Analysis Laboratory. 2020. High resolution land cover for City of Boston, MA (2019). Burlington, VT: University of Vermont Spatial Analysis Laboratory. https://bostonopendata-boston.opendata.arcgis.com/maps/boston::canopy-change-assessment-2019-land-cover/about

van Renterghem, T., Forssén, J., Attenborough, K., Jean, P., Defrance, J., Hornikx, M., & Kang, J. (2015). Using natural means to reduce surface transport noise during propagation outdoors. *Applied Acoustics*, *92*, 86–101. https://doi.org/10.1016/j.apacoust.2015.01.004

Venter, Z. S., Chakraborty, T., & Lee, X. (2021). Crowdsourced air temperatures contrast satellite measures of the urban heat island and its mechanisms. *Science Advances*, *7*(22). https://doi.org/10.1126/sciadv.abb9569

Vogt, J., Hauer, R., & Fischer, B. (2015). The costs of maintaining and not maintaining the Urban Forest: A review of the Urban Forestry and arboriculture literature. *Arboriculture & Urban Forestry*, *41*(6). https://doi.org/10.48044/jauf.2015.027

Wang, J. A., Hutyra, L. R., Li, D., & Friedl, M. A. (2017). Gradients of atmospheric temperature and humidity controlled by local urban land-use intensity in Boston. *Journal of Applied Meteorology and Climatology*, *56*(4), 817–831. https://doi.org/10.1175/jamc-d-16-0325.1

Wang, C., Wang, Z.-H., Wang, C., & Myint, S. W. (2019). Environmental cooling provided by urban trees under extreme heat and cold waves in U.S. cities. *Remote Sensing of Environment*, *227*, 28–43. https://doi.org/10.1016/j.rse.2019.03.024

Wang, J., Zhou, W., Jiao, M., Zheng, Z., Ren, T., & Zhang, Q. (2020). Significant effects of ecological context on urban trees' cooling efficiency. *ISPRS Journal of Photogrammetry and Remote Sensing*, *159*, 78–89. https://doi.org/10.1016/j.isprsjprs.2019.11.001

Wang, C., Ren, Z., Dong, Y., Zhang, P., Guo, Y., Wang, W., & Bao, G. (2022). Efficient cooling of cities at global scale using urban green space to mitigate urban heat island effects in different climatic regions. *Urban Forestry & Urban Greening*, *74*, 127635. https://doi.org/10.1016/j.ufug.2022.127635

Weinstein, N., Balmford, A., DeHaan, C. R., Gladwell, V., Bradbury, R. B., & Amano, T. (2015). Seeing community for the trees: The links among contact with natural environments, community cohesion, and crime. *BioScience*, *65*(12), 1141–1153. https://doi.org/10.1093/biosci/biv151

Weng, Q., Lu, D., & Liang, B. (2006). Urban surface biophysical descriptors and land surface temperature variations. *Photogrammetric Engineering & Remote Sensing*, *72*(11), 1275–1286. https://doi.org/10.14358/pers.72.11.1275

Winbourne, J. B., Jones, T. S., Garvey, S. M., Harrison, J. L., Wang, L., Li, D., Templer, P. H., & Hutyra, L. R. (2020). Tree transpiration and urban temperatures: Current understanding, implications, and future research directions. *BioScience*, *70*(7), 576–588. https://doi.org/10.1093/biosci/biaa055

World Health Organization. (2018, June 1). *Heat and health*. World Health Organization. Retrieved July 7, 2022, from https://www.who.int/news-room/fact-sheets/detail/climate-change-heat-and-health

Wynne, T., & Devitt, D. (2020). Evapotranspiration of urban landscape trees and turfgrass in an arid environment: Potential trade-offs in the landscape. *HortScience*, *55*(10), 1558–1566. https://doi.org/10.21273/hortsci15027-20

Yu, Q., Ji, W., Pu, R., Landry, S., Acheampong, M., O' Neil-Dunne, J., Ren, Z., & Tanim, S. H. (2020). A preliminary exploration of the cooling effect of tree shade in urban landscapes. *International Journal of Applied Earth Observation and Geoinformation*, *92*, 102161. https://doi.org/10.1016/j.jag.2020.102161

Zhu, Z., & Woodcock, C. E. (2012). Object-based cloud and cloud shadow detection in landsat imagery. *Remote Sensing of Environment*, *118*, 83–94. https://doi.org/10.1016/j.rse.2011.10.028

Zipper, S. C., Schatz, J., Kucharik, C. J., & Loheide, S. P. (2017). Urban heat island-induced increases in evapotranspirative demand. *Geophysical Research Letters*, *44*(2), 873–881. https://doi.org/10.1002/2016gl072190

Ziter, C. D., Pedersen, E. J., Kucharik, C. J., & Turner, M. G. (2019). Scale-dependent interactions between tree canopy cover and impervious surfaces reduce daytime urban heat

during summer. *Proceedings of the National Academy of Sciences*, *116*(15), 7575–7580. https://doi.org/10.1073/pnas.1817561116

Zivin, J., & Neidell, M. (2014). Temperature and the allocation of time: Implications for climate change. *Journal of Labor Economics*, *32*(1), 1–26. https://doi.org/10.1086/671766

Zhang, Y., Middel, A., & Turner, B. L. (2019). Evaluating the effect of 3D urban form on neighborhood land surface temperature using google street view and geographically weighted regression. *Landscape Ecology*, *34*(3), 681–697. https://doi.org/10.1007/s10980-019-00794-y

Zhou, D., Xiao, J., Bonafoni, S., Berger, C., Deilami, K., Zhou, Y., Frolking, S., Yao, R., Qiao, Z., & Sobrino, J. (2018). Satellite remote sensing of Surface Urban Heat Islands: Progress, challenges, and Perspectives. *Remote Sensing*, *11*(1), 48. https://doi.org/10.3390/rs11010048

Zhou, D., Xiao, J., Frolking, S., Zhang, L., & Zhou, G. (2022). Urbanization contributes little to global warming but substantially intensifies local and regional land surface warming. *Earth's Future*, *10*(5). https://doi.org/10.1029/2021ef002401

Zhou, W., Huang, G., & Cadenasso, M. L. (2011). Does spatial configuration matter? understanding the effects of land cover pattern on land surface temperature in urban landscapes. *Landscape and Urban Planning*, *102*(1), 54–63. https://doi.org/10.1016/j.landurbplan.2011.03.009

Zhou, W., Wang, J., & Cadenasso, M. L. (2017). Effects of the spatial configuration of trees on urban heat mitigation: A comparative study. *Remote Sensing of Environment*, *195*, 1–12. https://doi.org/10.1016/j.rse.2017.03.043

Figure & Table Captions

City	Latitude (°)	JJA Air Temperature (°C)	JJA Precipitation (mm)
Boston	42.4	22.0	263.9
Charlotte	35.2	25.8	306.7
Chicago	41.9	23.4	293.4
DC	38.9	24.0	304.3
Durham	36.0	24.4	372.6
San Diego	32.7	19.7	3.8
San Jose	37.3	20.5	5.8

Table 1. Mean summer (June, July, and August) air temperature (°C) and mean annual summer cumulative precipitation (mm) between 1991 and 2020 for the seven cities included in the analysis (National Centers for Environmental Information, 2022).

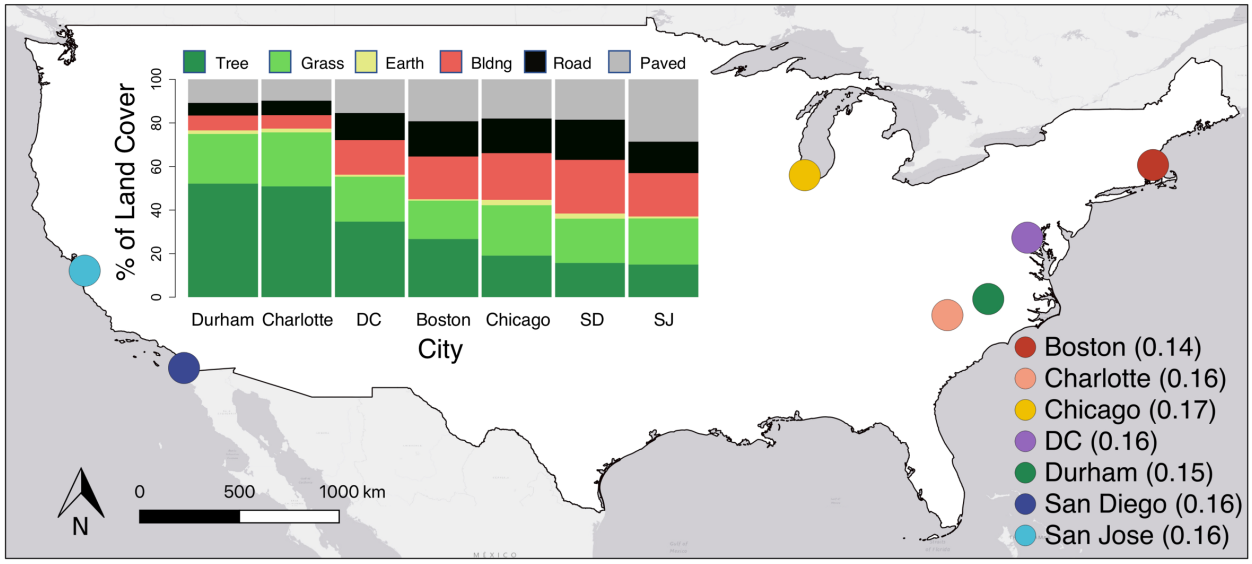

Figure 1. Map: Location of the seven cities included in the analysis. Numbers in the parentheses of the map legend represent the mean albedo of each city. Inset: Percent of each land cover type's contribution to total land area in each city sorted left-to-right by percent tree cover.

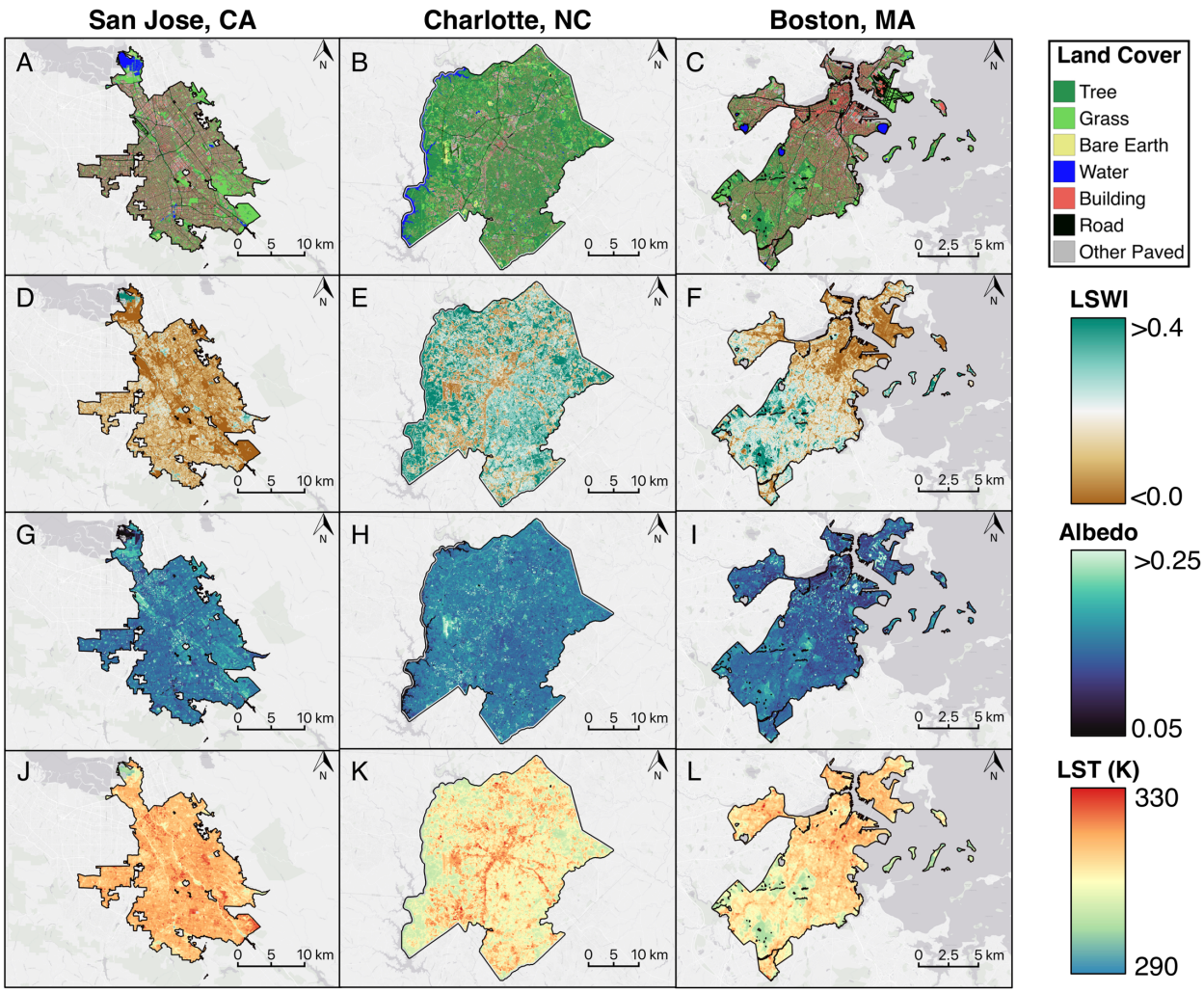

Figure 2. A-C: Land cover composition maps for Boston (2019), Charlotte (2012), and San Jose (2011). D-F: Five-year mean land surface water index (LSWI; unitless) raster composites for Boston (2015 – 2019), Charlotte (2008 – 2012), and San Jose (2007 – 2011). G-I: Five-year mean albedo (unitless) raster composites for Boston, Charlotte, and San Jose. J-L: Five-year mean land surface temperature (LST; K) raster composites for Boston, Charlotte, and San Jose. Land cover, LSWI, albedo, and LST data for Chicago, DC, Durham, and San Diego can be found in SI Figure 1.

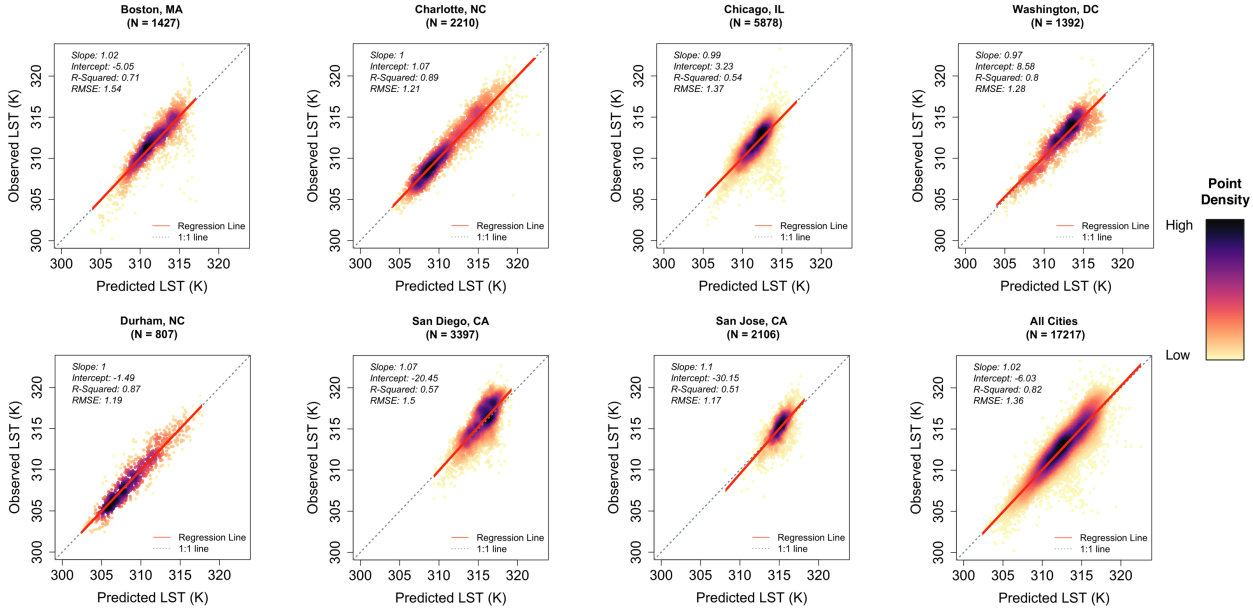

Figure 3. Observed LST (K) of the census blocks included within the testing datasets versus the predicted LST (K) of the census blocks in the testing dataset for all cities included in the analysis. N denotes the size of the testing dataset for each city.

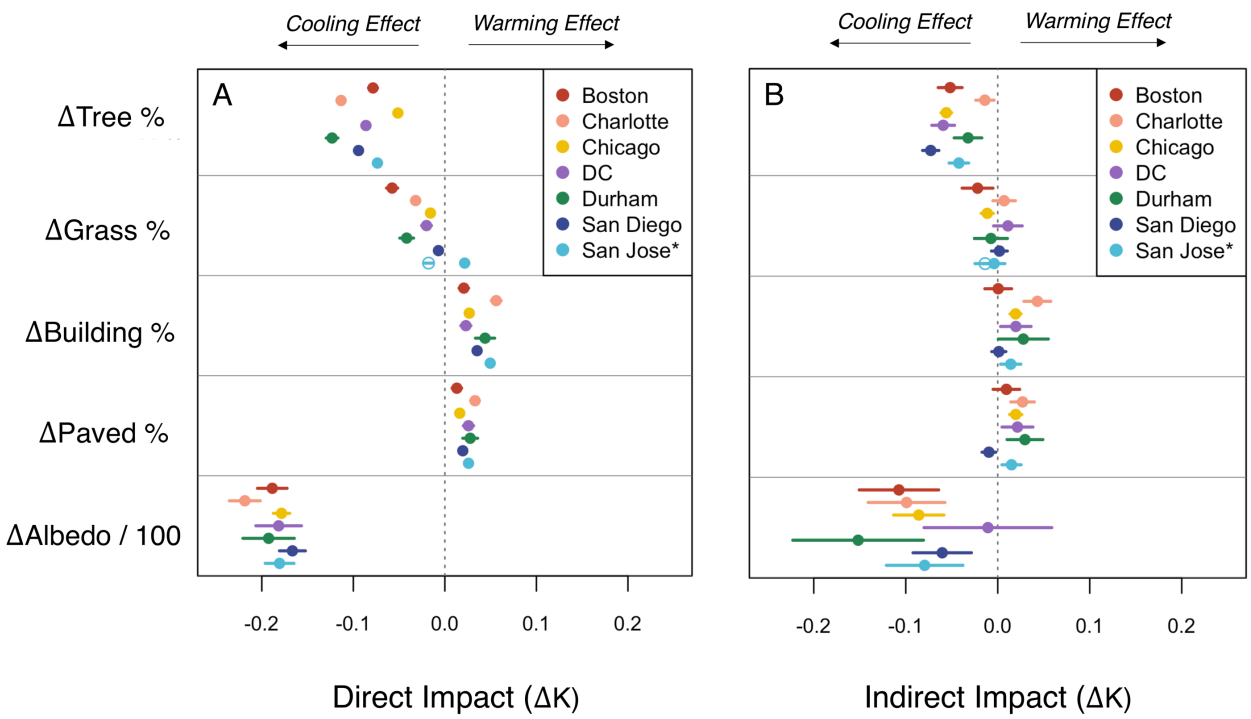

Figure 4. A: Direct impact coefficients estimated for each independent variable by each city-specific SDEM. *Irrigated grass cover in San Jose is designated by an open circle. Tree, grass, building, and paved cover coefficients should be interpreted as the change in surface temperature resultant from a one unit change in the percent land cover within a census block. Albedo coefficients should be interpreted as the change in surface temperature resultant from a 0.01 increase in the albedo within a census block. B: Indirect impact coefficients estimated for each independent variable by each city-specific SDEM. *Irrigated grass cover in San Jose is designated by an open circle. Tree, grass, building, and paved cover coefficients should be interpreted as the change in surface temperature resultant from a one unit change in the spatially weighted percent land cover in neighboring census blocks. Albedo coefficients should be interpreted as the change in surface temperature resultant from a 0.01 increase in the spatially weighted albedo of neighboring census blocks. All error bars represent 95% confidence intervals.

Direct Impacts and Intercepts						
City	**Tree %**	**Grass %**	**Building %**	**Other Paved %**	**Albedo/100**	**Intercept**
Boston	-0.079 ***	-0.058 ***	0.021 ***	0.013 ***	-0.189 ***	315.6 ***
Charlotte	-0.113 ***	-0.032 ***	0.056 ***	0.033 ***	-0.219 ***	318.9 ***
Chicago	-0.051***	-0.015 ***	0.027 ***	0.016 ***	-0.178 ***	314.5 ***
DC	-0.086 ***	-0.020 ***	0.023 ***	0.026 ***	-0.182 ***	316.3 ***
Durham	-0.123 ***	-0.042 ***	0.044 ***	0.028 ***	-0.193 ***	317.1 ***
San Diego	-0.094 ***	-0.007 ***	0.035 ***	0.020 ***	-0.167 ***	318.7 ***
San Jose	-0.074 ***	0.022 *** /*-0.018* ***	0.050 ***	0.026 ***	-0.181 ***	317.0 ***
Indirect Impacts and Spatial Error Coefficients						
City	**Tree %**	**Grass %**	**Building %**	**Other Paved %**	**Albedo/100**	**λ**
Boston	-0.052 ***	-0.022 *	0.0005	0.009	-0.107 ***	0.78 ***
Charlotte	-0.014 *	0.007	0.043 ***	0.027 ***	-0.099 ***	0.61 ***
Chicago	-0.056 ***	-0.011 ***	0.019 ***	0.020 ***	-0.086 ***	0.89 ***
DC	-0.060 ***	0.01	0.020 *	0.021 *	-0.011	0.76 ***
Durham	-0.032 ***	-0.0007	0.028 *	0.030 **	-0.152 ***	0.60 ***
San Diego	-0.073 ***	0.002	0.001	-0.009*	-0.060 ***	0.80 ***
San Jose	-0.042 ***	-0.003 /*-0.014* *	0.014 *	0.015**	-0.079 ***	0.76 ***

Table 2. Model intercepts, spatial error coefficients, and direct/indirect impact coefficients estimated for each independent variable by each city-specific SDEM, where irrigated grass cover in San Jose is designated by the italicized text. *** indicates statistical significance where $p < 0.001$, ** indicates statistical significance where $p < 0.01$, * indicates statistical significance where $p < 0.05$.

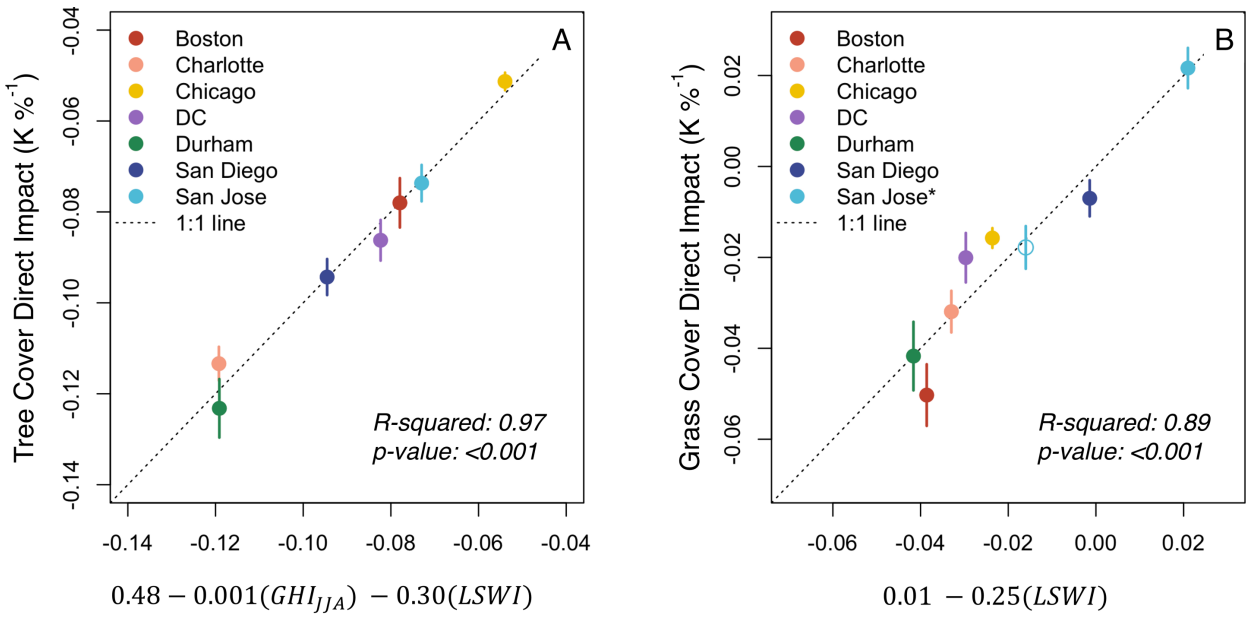

Figure 5. A: Tree cover direct impacts (K %-1) estimated from the SDEM for each city versus tree cover direct impacts (K %-1) estimated by a linear regression model predicting tree cover direct impacts as a function of mean JJA global horizontal irradiance (GHI; W m-2) and LSWI (unitless). B: Grass cover direct impacts (K %-1) estimated from the SDEM for each city versus grass cover direct impacts (K %-1) estimated by a linear regression model predicting grass cover direct impacts as a function of LSWI (unitless). *For San Jose, irrigated grass cover is designated by an open circle and non-irrigated grass cover is designated by a closed circle. All error bars represent 95% confidence intervals.

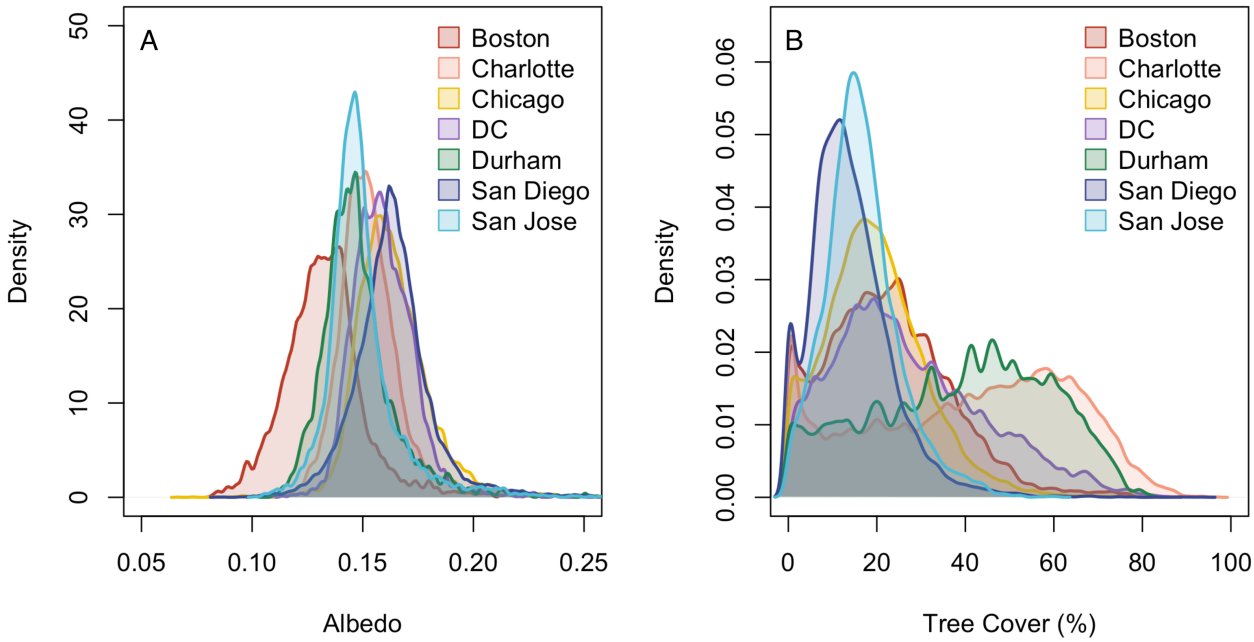

Figure 6. A: Kernel density distribution of albedo at the census block level for each city included in the analysis. B: Kernel density distribution of tree cover (%) at the census block level for each city included in the analysis.

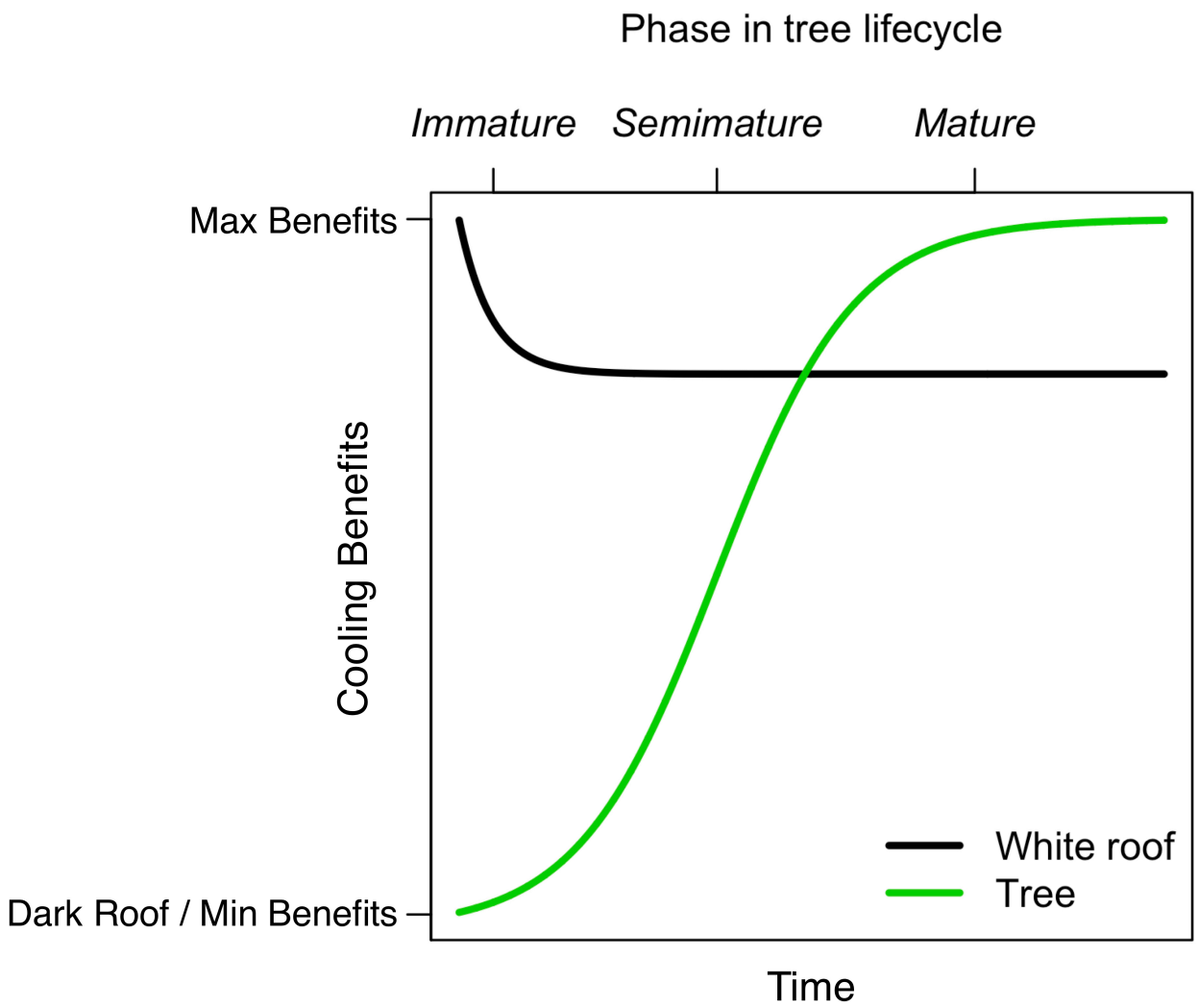

Figure 7. Conceptualization of the temporal evolution of cooling benefits provided by trees versus white roofs (Adapted from data and figures in Bretz & Akbari 1997 and Vogt et al. 2015).

Supplemental Information

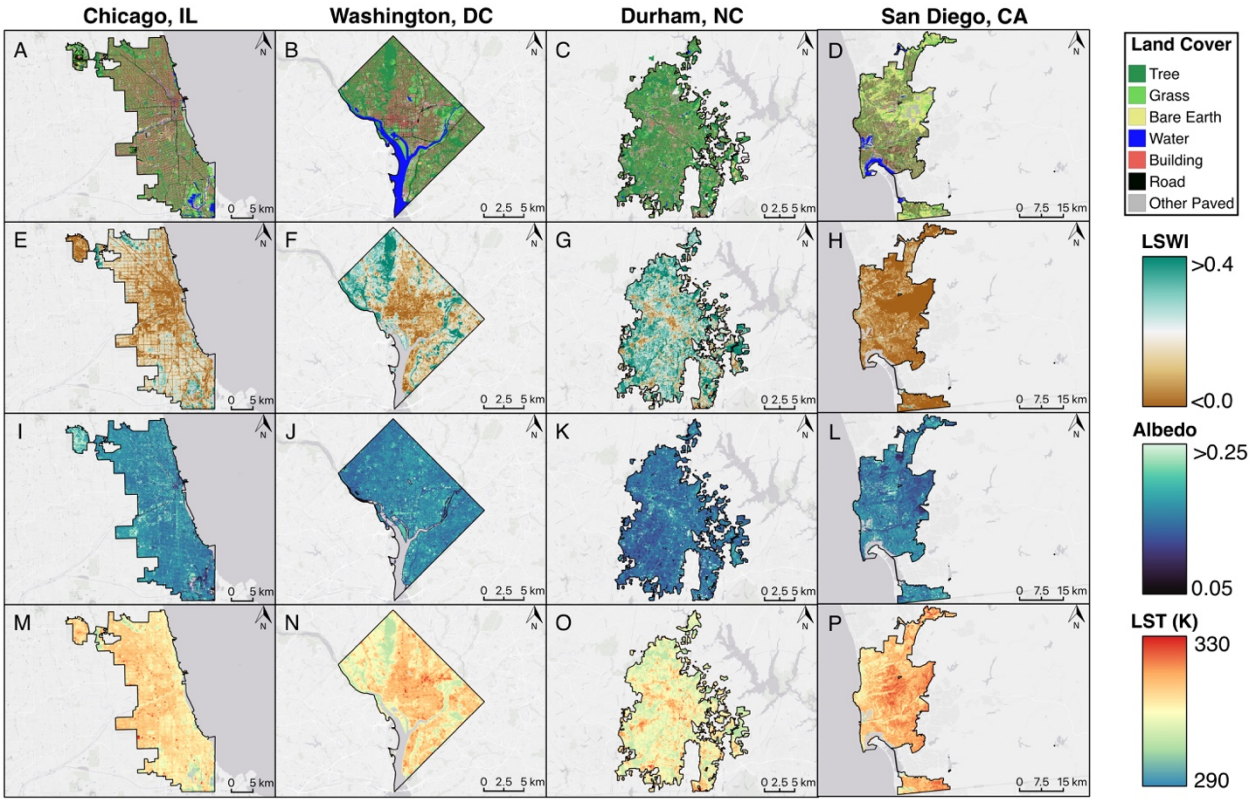

SI Figure 1. A-D: Land cover composition maps for Chicago (2010), DC (2011), Durham (2015), and San Diego (2017). E-H: Five-year mean land surface water index (LSWI; unitless) raster composites for Chicago (2006 – 2010), DC (2007 – 2011), Durham (2011 - 2015), and San Diego (2013 – 2017). I-L: Five-year mean albedo (unitless) raster composites for Chicago, DC, Durham, and San Diego. M-P: Five-year mean land surface temperature (LST; K) composites for Chicago, DC, Durham, and San Diego.

980
981
982 **SI Table 1.** Inventory of Landsat images used to create the five-year JJA clear sky raster composites of surface temperature,
983 albedo, and LSWI.

City	Year	Images
Boston (n = 23 images)	*2015*	LE07_012031_20150617, LE07_012031_20150703, LE07_012031_20150719, LE07_012031_20150804, LE07_012031_20150820
	2016	LE07_012031_20160619, LE07_012031_20160721, LE07_012031_20160806, LE07_012031_20160822
	2017	LE07_012031_20170622, LE07_012031_20170708, LE07_012031_20170809, LE07_012031_20170825
	2018	LE07_012031_20180609, LE07_012031_20180625, LE07_012031_20180711, LE07_012031_20180727, LE07_012031_20180828
	2019	LE07_012031_20190612, LE07_012031_20190628, LE07_012031_20190730, LE07_012031_20190815, LE07_012031_20190831
Charlotte (n = 22 images)	*2008*	LE07_017036_20080616, LE07_017036_20080702, LE07_017036_20080718, LE07_017036_20080803, LE07_017036_20080819
	2009	LE07_017036_20090603, LE07_017036_20090619, LE07_017036_20090721, LE07_017036_20090806, LE07_017036_20090822
	2010	LE07_017036_20100606, LE07_017036_20100622, LE07_017036_20100708, LE07_017036_20100724, LE07_017036_20100809
	2011	LE07_017036_20110609, LE07_017036_20110625, LE07_017036_20110711,

		LE07_017036_20110727, LE07_017036_20110828
	2012	LE07_017036_20120627, LE07_017036_20120729,
Chicago (n = 20 images)	*2006*	LE07_023031_20060605, LE07_023031_20060707, LE07_023031_20060723, LE07_023031_20060824
	2007	LE07_023031_20070608, LE07_023031_20070710, LE07_023031_20070726, LE07_023031_20070811,
	2008	LE07_023031_20080610, LE07_023031_20080626, LE07_023031_20080728, LE07_023031_20080813, LE07_023031_20080829
	2009	LE07_023031_20090715, LE07_023031_20090731,
	2010	LE07_023031_20100616, LE07_023031_20100702, LE07_023031_20100718, LE07_023031_20100803, LE07_023031_20100819
DC (n = 21 images)	*2007*	LE07_015033_20070616, LE07_015033_20070702, LE07_015033_20070718, LE07_015033_20070803,
	2008	LE07_015033_20080602, LE07_015033_20080618, LE07_015033_20080704, LE07_015033_20080720, LE07_015033_20080821
	2009	LE07_015033_20090707, LE07_015033_20090808, LE07_015033_20090824
	2010	LE07_015033_20100608, LE07_015033_20100824, LE07_015033_20100726, LE07_015033_20100811, LE07_015033_20100827
	2011	LE07_015033_20110611, LE07_015033_20110713, LE07_015033_20110729, LE07_015033_20110830
Durham (n = 22 images)	*2011*	LE07_016035_20110602,

		LE07_016035_20110618, LE07_016035_20110720, LE07_016035_20110821
	2012	LE07_016035_20120604, LE07_016035_20120620, LE07_016035_20120706, LE07_016035_20120823
	2013	LE07_016035_20130623, LE07_016035_20130810, LE07_016035_20130826
	2014	LE07_016035_20140610, LE07_016035_20140626, LE07_016035_20140712, LE07_016035_20140728, LE07_016035_20140813, LE07_016035_20140829
	2015	LE07_016035_20150613, LE07_016035_20150629, LE07_016035_20150715, LE07_016035_20150731, LE07_016035_20150816
San Diego (n = 28 images)	*2013*	LE07_040037_20130615, LE07_040037_20130701, LE07_040037_20130717, LE07_040037_20130802, LE07_040037_20130818
	2014	LE07_040037_20140602, LE07_040037_20140618, LE07_040037_20140704, LE07_040037_20140720, LE07_040037_20140805, LE07_040037_20140821
	2015	LE07_040037_20150605, LE07_040037_20150621, LE07_040037_20150707, LE07_040037_20150723, LE07_040037_20150808, LE07_040037_20150824
	2016	LE07_040037_20160623, LE07_040037_20160709, LE07_040037_20160725, LE07_040037_20160810, LE07_040037_20160826
	2017	LE07_040037_20170610, LE07_040037_20170626, LE07_040037_20170712,

		LE07_040037_20170728, LE07_040037_20170813, LE07_040037_20170829
San Jose (n = 25 images)	2007	LE07_044034_20070611, LE07_044034_20070627, LE07_044034_20070713, LE07_044034_20070729, LE07_044034_20070814, LE07_044034_20070830
	2008	LE07_044034_20080629, LE07_044034_20080715, LE07_044034_20080731, LE07_044034_20080816
	2009	LE07_044034_20090616, LE07_044034_20090702, LE07_044034_20090718, LE07_044034_20090803, LE07_044034_20090819
	2010	LE07_044034_20100603, LE07_044034_20100619, LE07_044034_20100705, LE07_044034_20100721, LE07_044034_20100822
	2011	LE07_044034_20110622, LE07_044034_20110708, LE07_044034_20110724, LE07_044034_20110809, LE07_044034_20110825

SI Table 2. Summary of census blocks filtered from the analysis due to the minimum area requirement (3600 m^2).

City	Census blocks with >1% building cover	Census blocks with > 1% building cover and > 3600 m^2	Median area of census blocks in analysis (m^2)
Boston	5285	4755	12687
Charlotte	7532	7366	40930
Chicago	20083	19594	20427
DC	4910	4641	16437
Durham	2721	2690	32451
San Diego	12134	11322	13547
San Jose	7395	7020	24938

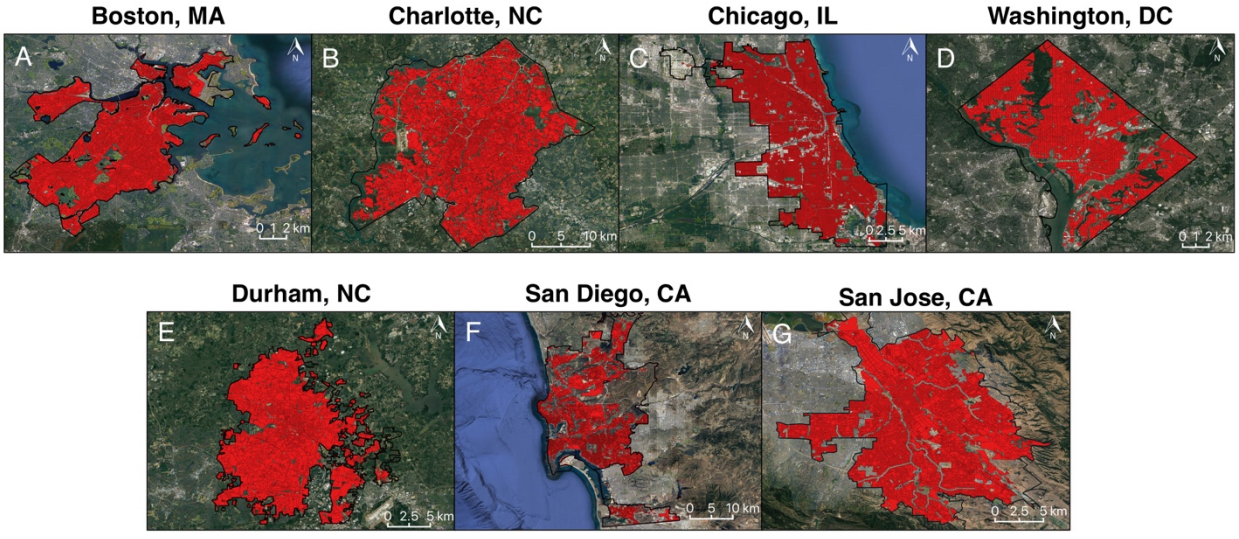

SI Figure 2. Census blocks included in the SDEM analysis for each city after application of water, area, and landcover filters.

SI Table 3. Variance inflation factor (VIF) of all variables included in each city-specific SDEM where the VIF for irrigated grass cover in San Jose is designated by italicized text.

City	Tree %	Grass %	Building %	Other Paved %	Albedo
Boston	3.67	2.51	4.79	3.03	1.07
Charlotte	9.56	5.22	3.15	5.62	1.24
Chicago	2.32	2.19	2.28	2.92	1.14
DC	5.55	2.92	4.23	3.49	1.39
Durham	7.00	2.91	2.20	3.97	1.42
San Diego	1.96	2.38	1.85	2.79	1.21
San Jose	1.87	2.08/*1.50*	2.06	2.05	1.32

SI Table 4. Moran's I statistic quantifying the correlation of SDEM residuals and spatially-lagged SDEM residuals, and the associated p-values for a two-sided Moran's I test conducted on the SDEM residuals for each city. P-values > 0.05 indicate no significant spatial autocorrelation of SDEM residuals.

City	Moran's I Statistic	p-value
Boston	-0.0003	0.99
Charlotte	-0.005	0.48
Chicago	0.005	0.16
DC	-0.010	0.24
Durham	-0.001	0.97
San Diego	-0.002	0.74
San Jose	-0.011	0.14